Università degli Studi di Milano

FACOLTÀ DI SCIENZE E TECNOLOGIE
Corso di Laurea in Fisica

Corso di Laurea Triennale in Fisica

Neutron stars as probes of the nuclear Equation of State

Candidato:
Bolis Manuel
Matricola 944083

Relatore:
Gianluca Colò

Correlatore:
Xavier Roca Maza

Anno Accademico 2021-2022

Index

Chapter 1

Introduction

Neutron stars are among the most exotic objects in our universe. Their density can reach several times the one found in normal atomic nuclei, so they are by all means the most compact stars known. As far as observed to date, their mass ranges between ~ 1.4 and ~ 2.50 solar masses ($M_\odot = 1.989 \times 10^{33}$ g), within a radius of about 10 km. In comparison, black holes have masses in the range of about 3 to 70 solar masses and a radius equal to the Schwarzschild radius ($R_S = 2GM/c^2$).Despite their name, neutron stars are not composed only of neutrons; rather, protons, electrons, muons and other more exotic particles are also present within them.At the high densities present in its inner core, in fact, it is thought that more massive particles such as hyperons may appear, or even that matter may occur in the form of deconfined quarks.

Neutron stars are objects of deep and current interest, as their understanding involves all the known four forces. They represent an exceptional laboratory for investigating matter at ultrahigh densities, in no way attainable on Earth. Their stability rests on a perfect balance between gravity and the pressure generated by matter due to the Pauli exclusion principle and the strong interaction.

Landau was the first to hypothesize the existence of extremely dense stars in an article written in 1931 [1], although in it he never explicitly referred to a neutron star. In this paper Landau, who was only 23 years old at the time, finds a simple formula for the maximum mass of white dwarfs in a manner independent of the similar result found by Chandrasekhar. In the second half of the article, however, Landau goes further by hypothesizing stars of higher density, for which the laws of quantum mechanics would have ceased to apply. His conclusion, referring to such high density stars, was: *"the density of matter becomes so great that atomic nuclei come in close contact, forming one gigantic nucleus"*.

The extraordinary fact is, as reported in the article [2], that Landau's idea took shape even before Chadwick's discovery of the neutron (1932). However, the term "neutron star" was coined by the two physicists Walter Baade and Fritz Zwicky in 1933. They first proposed, speculatively, the existence of such stars in connection with the phenomenon of supernovae, dying stars that in a violent explosion release a very high amount of energy, the brightness of which comes to overpower for a period of several days or weeks that of an entire galaxy.

In this thesis work, we are interested in investigating the nuclear physics aspects that are related to the high-density matter forming these objects.

The central issue regarding neutron stars consists of the study of the "Equation of

State" (EoS) for high-density matter. It represents a relationship between energy density and pressure and is highly dependent on the theoretical model with which it is studied. To date, there is no definitive EoS that can describe matter over the wide range of densities present in a neutron star (up to 10^{15} g cm^{-3}). Several attempts have been made to construct unified equations of state, while another possibility consists in studying the equation of state of matter in different density ranges and then combining the various building blocks into a single relation. In this work, the second solution was opted for, namely we have chosen the merging between two models, specifically the one proposed by Baym, Pethick and Sutherland (BPS) (1971) and a model based on Skyrme-type interactions within the framework of mean-field theories.

Once an EoS is available, it is possible to solve the TOV equation (Tolman, Oppenheimer and Volkoff), that is, the equations for the hydrostatic equilibrium of a spherical symmetry body subject to its own gravity, consistent with general relativity. Indeed, in order to have a closed system of differential equations the TOV must be supported by an appropriate equation of state.

To solve such equations it is necessary to implement a suitable numerical code and this work is mainly devoted to that task. The results consists in a mass-radius relation for neutron stars to be compared with the astrophysical observations available to date [3; 4; 5; 6].

In this way neutron stars, which belong to the large scales of astrophysics can surprisingly constitute a valid test to verify the goodness of the equation of state that describes microscopic matter.

Thanks to the possibility of detecting and analyzing gravitational waves, whose sources can sometimes be neutron stars in binary systems, it is also possible to test an additional parameter predictable by theoretical models, namely the tidal deformability [7]. The latter quantifies the capability of an object to deform under the effect of a gravitational field produced for example by a companion object in a binary system. It is easy to guess how the tidal deformability of a compact object is closely related to the matter of which it is composed and for this reason it constitutes another valid test for the equation of state.

Finally, by putting together the different analyses made for the observable mass, radius and tidal deformability, considerations can be drawn on the validity of the various models tested within the hypotheses with which they were built.

In particular, after testing our code on EoS models widely used in literature, analyses have been conducted on EoSs created by implementing Skyrme functionals built by nuclear physics group in Milan. Finally, the same analyses have been carried out on a model proposed by S. A. Fayans in 1998, which is currently heavily studied in the field of nuclear physics but has not yet been applied to the study of neutron stars.

Chapter 2

Structure and observed properties of neutron stars

Neutron stars have a complex structure and many of their aspects remain to this day an open question of wide interest to the scientific community. The study of these compact objects provides fundamental insights into the understanding of matter under high-density conditions that are impossible to achieve in a laboratory on Earth. The huge density variation in the range $\sim 10^{11} - 10^{15}$ g/cm^{-3} expected in neutron stars requires the modelling of systems in very different physical conditions.
Figure 2.1 encapsulates our current knowledge about the structure and composition of a neutron star, a topic that will be treated in this chapter following a layered description.
Then at the end of this chapter the main astrophysics observations will be mentioned, which provide an important test for the predictions of our models.

2.1 Inside a neutron star: layers and structure

According to current understanding of neutron stars, they can be subdivided into the *atmosphere* and four main internal regions: the *outer crust*, the *inner crust*, the *outer core* and the *inner core*.
The atmosphere is composed of a thin plasma layer where the spectrum of the thermal electromagnetic neutron star radiation is formed. This layer has some relevance since assuming the star as a black body an estimate of surface temperature can be computed ($T_s = 10^6 K$). This layer is only few millimeters thick and its contribution to the total mass is negligible.
For the purposes of this work we are most interested in the 4 innermost levels for which we provide a more in-depth description.

2.1.1 The outer crust

This region has a thickness between 0.3 and 0.5 km, and is composed of matter with density $\rho < \rho_{drip} \simeq 4 \times 10^{11}$ g cm^{-3}, where ρ_{drip} is the density of the so-called "drip point" at which nuclei are no longer able to hold additional neutrons [9; 10]. At such a density, the matter is composed of a Coulomb lattice of nuclei surrounded by a gas

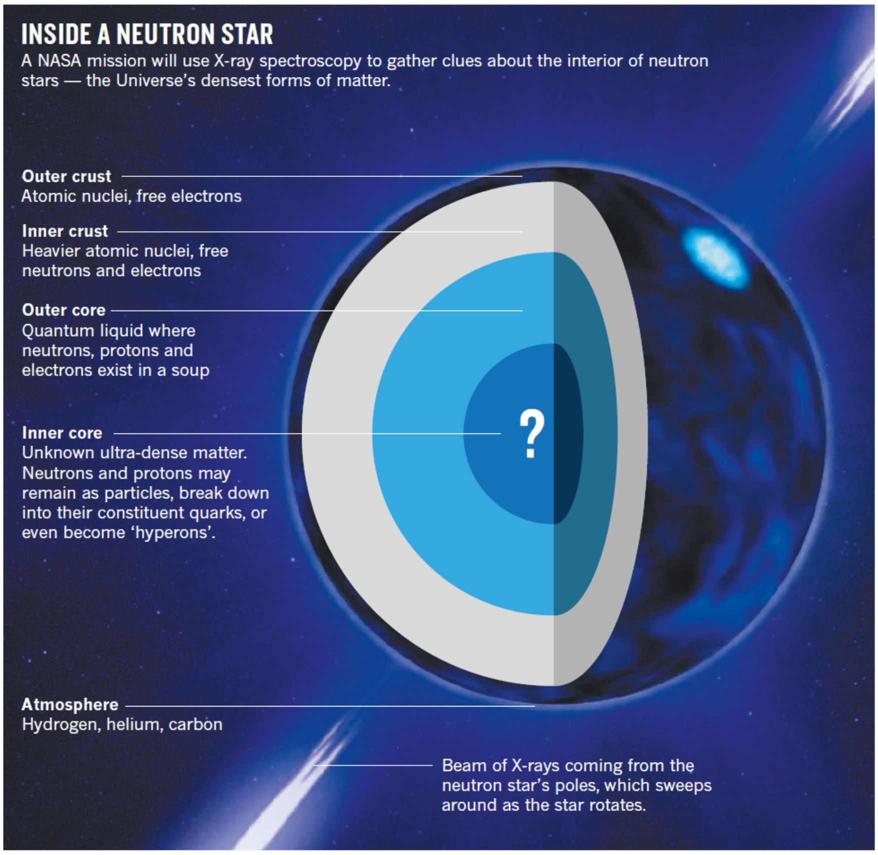

Figure 2.1: Pictorial representation of the structure of a neutron star, published on Nature [8] on the occasion of the start of Nasa's NICER mission (2017) .

of electrons. Furthermore the densities are high enough to ionize the atoms and thus nuclei see the electric charge of their neighbors and arrange in a Coulomb lattice. It should also be noted that electrons are ultra-relativistic starting from a density $\rho = 10^6$ g cm^{-3}. The largest contribution to the pressure is due precisely to the electrons. The ground state of matter at this density was first described by Baym et al. (1971) [11] as the configuration for which the energy per nucleon $E = \mathcal{E}/n_b$ is minimized , where n_b is the total baryonic density. We will henceforth refer to the equation of state (EoS) they proposed by the acronym BPS.

Noting that n_b is not a good parameter since it is discontinuous as one proceeds into the interior of a neutron star, a better description is given using the pressure P as the variable. The latter has to be a continuous function of r (distance from the centre), to ensure mechanical stability of the star. In this way the ground state configuration is the one that minimizes the Gibbs free energy $h = (\mathcal{E} + P)/n_b$. For example, in the outermost parts of the star where $P \sim 0$, and the Gibbs free energy is identified with E/A it is easy to see that the most stable configuration is made with ^{56}Fe nuclei.

In their article [11], BPS consider matter arranged in a lattice structure composed of individual Wigner-Seitz cells containing a single nucleus. The Gibbs free energy for each cell $G_{cell}(A, Z)$ depends on the mass number A and the atomic number Z and is

composed of three terms: i) the nuclear energy (including rest energy), ii) the lattice energy contribution, which is a measure of the binding energy of the crystal structure due to Coulombic interactions, iii) electron energy.
Having accurate tables of nuclear masses (measured in the laboratory), it is possible to calculate, for each value of pressure P, which is the optimal nucleus, minimizing the Gibbs free energy per nucleon $h = G_{cell}/A$ with respect to A and Z (mass number and number of protons of the nucleus, respectively). It should be noted that these tables are constructed with experimental data only up to a certain point, after which favored nuclei have never been measured. Therefore, a theoretical model is needed.
We then see that at different values of pressure (density) the ^{56}Fe nucleus is no longer the most convenient. This is due to the fact that as the density increases, the electronic contribution to the Gibbs free energy tends to increase significantly; it therefore becomes energetically convenient for the system to convert electrons into neutrons, by means of electron capture. Proceeding toward ρ_{drip} will thus result in increasingly neutron rich nuclei. For many models this sequence ends with ^{118}Kr, a nucleus composed of 36 protons and 82 neutrons.

2.1.2 The inner crust

The inner crust extends for about $1 - 2$ km [9; 10] and has a density that varies between ρ_{drip} to about one-half of the saturation density $\rho_0 = 2.8 \times 10^{14}$ g cm^{-3} ($n_b = 0.15$ fm^{-3}). In this region highly neutron-rich nuclei are immersed in a neutron gas in a superfluid state. The exact form of the nucleon-nucleon (NN) interaction is poorly known, so a theoretical approach, based on many-body theory, must be used. One possible technique is based on Hartree-Fock type calculations, on which the model of Skyrme-type interactions used in this work is also based. In the higher levels of the inner crust, the distances between the nuclei are still large enough that the Coulombic interaction (long-range repulsive) and strong interaction (short-range attractive) do not interfere with each other, allowing the material to maintain its structure. However, as one moves towards the inner levels and the density increases, the interparticle distances shorten. This causes the Coulombic and strong interactions to begin to compete with each other, which leads to what is known as "Coulomb frustration." This phenomenon leads to the formation of special nuclear structures, known as nuclear pasta, because of the various geometries that precisely resemble various types of pasta.

2.1.3 The outer core

The outer core occupies a density range of $0.5\rho_0 \leq \rho \leq 2\rho_0$ and is several kilometers thick. Its matter is composed mostly of neutrons with the addition of a certain fraction of protons, electrons are also needed in order to have charge neutrality. As one progressively moves towards the innermost layers of the star and at a certain threshold density dependent on the model used, muons μ also appear. Their presence is justified by the fact that for matter at high densities, slow muons becomes more energetically favorable rather than electrons, as the energy due to their fermionic nature increases rapidly with density.
The matter just described, hereafter referred to as $npe\mu$ matter, must also satisfy the condition of equilibrium with respect to weak interactions (β-equilibrium), the details of which will be discussed in depth in subsequent chapters. In this model,

electrons and muons form an ideal Fermi gas, while protons and neutrons constitute a strongly interacting Fermi liquid, which in this work will be described by Skyrme-type interactions within the framework of non-relativistic mean-field theories.

2.1.4 The inner core and the hyperon puzzle

The inner core is the central region of a neutron star; its extension and the properties of the matter composing it are poorly understood to date. Typically, the baryonic densities reached in this part of the neutron star lie in a range from $\sim 2\rho_0$ up to very high values $(10 - 15\rho_0)$ [10].
Several hypotheses have been formulated to describe matter under these extreme conditions, two of them being: i) the hypothesis of a hyperonization of matter, i.e., the appearance of hyperons, first of all Λ and Σ^-, ii) a quark matter phase transition, consisting of deconfined u, d, s quarks.
The reason hyperons are present at high densities is due to the fermionic nature of nucleons. The energy of protons and neutrons grows rapidly as density increases (Fermi model) and at a certain threshold it is energetically more convenient for neutrons closer to the Fermi surface to decay into Λ particles.
In addition under normal density conditions, such as those in a laboratory on earth, Λ particles are unstable and would decay in a very short time, but under high density conditions they stabilize due to the Pauli exclusion principle that prevents their decay, hence a certain fraction of Λ can be present in conditions of equilibrium. Similarly, Σ^- particles can be produced by reactions of the type $e^- + n \to \Sigma^- + \bar{\nu}_e$.
The addition of hyperons in the nuclear matter model leads to a drastic decrease in the maximum mass supportable by such a system, with consequent results in strong disagreement with astrophysical observations of neutron stars. This issue is known in the literature as the "hyperon puzzle." Works such as [12] show results that exemplify what has just been said and advance some hypotheses for overcoming this problem. In general, the difficulties of this model in predicting experimental observations can be attributed to the lack of knowledge of hypernuclear matter, the study of which is a very active field to date. The instability of hyperons under laboratory conditions, makes scattering experiments particularly difficult. Today very little is still known about the nucleon-hyperon type interaction, and even less is known about the interaction between hyperons [13]. In order to better understand the behavior of matter in the presence of hyperons, in addition to scattering experiments, it is useful to know the binding energy of hypernuclei (nuclei in which some nucleons are replaced by hyperons); to date, measurements are available only for some light hypernuclei (atomic mass $A = 3, 4$).

Therefore, given the limited knowledge about this configuration of matter, hyperons will not be considered in this thesis work. Instead, the Skyrme-type model used to describe the matter of the inner crust and outer core will be extended to the high densities expected in the inner core.

2.2 Constraints from astrophysical observations

We have already mentioned the fact that the study of neutron stars is an interdisciplinary topic at the border between the fields of astrophysics and nuclear physics. By utilizing evidence from astrophysical observations, we can place constraints on the results obtained from a specific nuclear equation of state. There are available measurements of radii, masses, and tidal deformabilities of certain neutron stars, which can be used to compare the results obtained from the equation of state with the observed data. Such an analysis is helpful in determining the efficacy of a particular equation of state, see ref [9] for an up to date review. In this section we'll summarize some of the most important astrophysical observations for neutron stars.
Using the Newtonian theory of gravity it is only possible to determine the combined mass of a binary system be means of Kepler's third law:

$$P^2 = \frac{4\pi^2}{G(M_1 + M_2)} a^3, \tag{2.2.1}$$

where P is the orbital period, a is the length of the semi-major axis of the ellipse and M_1 and M_2 are the individual masses. In order to break such a degeneracy one has to invoke once again General Relativity. Indeed, one important approach used to determine the mass of a neutron stars in a binary system is that of pulsar timing together with the Shapiro delay.
Most of neutron stars are observed as pulsars, whose name comes from the fact that they look like a "lighthouse". These objects are fast-spinning neutrons stars emitting beams of electromagnetic radiation out of their poles, the "lighthouse" effect is generated by the combination of these beams together with the rotation as observed from the Earth. The period of this pulsation is so constant in time that astronomers refer to pulsars as the most precise clocks in the Universe.
The Pulsar timing method [14] consists in a detailed study of the TOA ("Time of Arrival") of the signals from a neutron star. Simplifying, using data analysis and noise removal techniques departing from raw data, one obtains a TOA that is compared to an arrival time predicted using a timing model that includes all astrometric parameters. Some of these parameters are pulsar's position, proper motion, and parallax, all possible binary parameters, dispersion delays, and the pulsar slowdown. The deviations between those two times are minimized by a least-squares fit for the timing model parameters, what's left are "post-fit residuals" that are inspected for possible systematic trends that may, for instance, reflect the effect of an unmodeled variable of the system. Another tool use in the investigation of neutron star properties exploit a phenomena known as Shapiro delay (one of the main tests of General Relativity, i.e., the bending of light traveling near a massive object) of the radio signal due to the companion planet, and thus used to infer the mass of the latter. In this way the degeneracy of mass described above is broken and eventually the mass of the neutron star can be determined.
This technique was used back in 2010 to determine the mass of the pulsar $PSRJ1614-2230$ $(1.97 \pm 0.04 M_\odot)$ [15], the most massive known back then. Before NICER (Neutron Star Interior Composition Explorer) launch in 2017, joint measurements of mass and radius of a neutron stars were not possible, so in a sense with this project NASA started a new age for observational astrophysics of neutron stars. From the International Space Station (ISS) NICER, which relies on a sophisticated investigation method known as Pulse Profile Modeling, measured for the first time the mass and ra-

Table 2.1: Main results from astrophysical observations

Pulsar	**Mass** [$M_\odot$]	**Radius** [km]
PSRJ1614-2230	1.97 ± 0.04	
PSRJ0030+0451 [3]	$1.44^{+0.15}_{-0.14}$	$13.02^{+1.24}_{-1.06}$
PSRJ0030+0451 [16]	$1.34^{+0.15}_{-0.16}$	$12.71^{+1.14}_{-1.19}$
PSRJ0740+6620	2.08 ± 0.07	12.39 ± 1.15
PSRJ0952-0607	2.35 ± 0.17	

dius of a neutron star, namely $PSRJ0030{+}0451$. Two independent studies on NICER data have found two slightly different results: ($1.44^{+0.15}_{-0.14}M_\odot$, $R = 13.02^{+1.24}_{-1.06}$ km) [3], and ($1.34^{+0.15}_{-0.16}M_\odot$, $R = 12.71^{+1.14}_{-1.19}$ km) [16] respectively. NICER measured also the mass record holder until July 2022 $PSRJ0740-6620$ ($2.08\pm0.07M_\odot$,$R = 12.39\pm1.15$ km) [4]. These two pioneering results suggested that the equation of state in the relevant density domain must be pretty "stiff", indeed a stiffer EoS means more pressure for a fixed value of energy density and as a consequence more resistance to compression and support against gravity resulting in larger radii and higher masses [9].
At the present date the most massive well-measured neutron star with a confidence of 90% on the mass estimate is $PSRJ0952-0607$ “The Fastest and Heaviest Known Galactic Neutron Star” [6], which orbit in a “spider binary” (the name that astronomers use to give to a system in which the neutron stars behave like a “black widow” spider slowly absorbing the companion mass until its complete disruption), that is as massive as $2.35M_\odot$, within an error of $\pm0.17M_\odot$.
On the other hand, with the beginning of the age of gravitational waves, an international collaboration between LIGO and VIRGO laboratories provided some other very important results. As will be described in detail below, the tidal deformability of a neutron star, namely a constant that describes the tendency of a neutron star to develop a mass quadrupole response to the tidal field induced by its companion, is one of the observables that can be a priori calculated once an EoS is selected. As described in the section on tidal deformability, in the wave signal is someway encoded information about the masses and tidal deformability Λ of the two components of a binary system.
As soon as the first NS-NS merging gravitational wave detection ($GW170817$), a constraint on the tidal deformability of a slow-spin neutron star was found [7], that is $\Lambda_{1.4M_\odot} \leq 800$. Further studies deduced a lower and an upper limit on the radius of a 1.6M$\odot$ neutron star for which R $>$ 10.68 km [5; 17] and of a 1.4M$\odot$ neutron star for which R $<$ 13.76 km respectively, this limits implies a soft EoS in higher density regions, resulting in smaller radii.
In contrast to what is observed by NICER, whose results suggest a quite stiff EoS, gravitational waves constraint for a $1.4M_\odot$ neutron star predicts a radius $R = 11.40^{+1.38}_{-1.04}$ [18], a lower value than that measured by NICER for a star of the same mass. A lower radius is indicative of a softer EoS as described above, therefore this last result is one of the very few which indicates the EoS is soft.
In conclusion we remark the interesting fact that this results, owing to the very large scales of the astrophysics, represent a key factor in the study of the microscopical domain of neutron-rich matter, constraining and potentially validating nuclear physics calculations, for instance by means of Bayesian inference [19].

Chapter 3

Physics of neutron stars

Understanding neutron stars requires a broad set of notions, pertaining to different fields of Physics, from general relativity to microscopical structure of nuclear matter. In this chapter, we discuss the theoretical models on which our results were based. In particular, we will discuss the foundations of hydrostatic equilibrium in general relativity, the tidal deformability and how it is extrapolated from gravitational wave data, and finally some models that can describe nuclear matter. These models are widely used and have proven to be effective tools for understanding nuclei and their properties.

3.1 Tolmann-Oppenheimer-Volkoff (TOV) Equations

A neutron star represents a possible final stage in stellar evolution, in particular it's what's left of a collapsed core of a massive supergiant star, which had a total mass of between 10 and 25 solar masses. We can naturally assume stars as spherically symmetric objects in hydrostatic equilibrium (as long as rotation is not taken into account), i.e. in a condition such that gravity due to the mass of the object itself is equilibrated by some pressure. A star like the Sun generates pressure through nuclear fusion, which counteracts the force of gravity and supports the star against collapse. This process of generating pressure through nuclear fusion continues as long as the star has fuel to burn. When a star exhausts its fuel, the balance between pressure and gravity is disrupted, and the star's fate is determined by its mass.
In more exotic stars such white dwarfs or neutron stars, made of degenerate matter, pressure has to do with quantomechanical properties, such as Pauli exclusion principle, and interactions between nucleons at high densities.
One trivial approach is to derive hydrostatic equilibrium in Newtonian mechanics which fails, by the way, to describe neutron stars as they come in a context where gravity is extreme and General Relativity is no longer negligible.
First consider a thin shell of thickness dr of a sphere (see Figure 3.1) , its mass is equal to $\rho\left(r\right)4\pi r^2 dr$, then compute the gravitational force between this shell and the total mass $m(r)$ between 0 and r

$$dF = -\frac{Gm\left(r\right)\rho\left(r\right)4\pi r^2 dr}{r^2}. \tag{3.1.1}$$

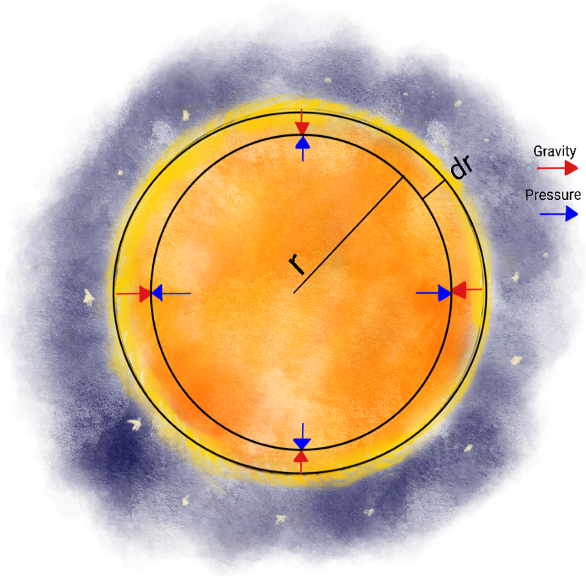

Figure 3.1: Pictorial representation of the hydro-static equilibrium between pressure and gravity for a general star.

Dividing it by $4\pi r^2$ we get the inward pressure due to the gravitational force, that has to be equal to $p(r) - p(r+dr)$ that is the difference between the internal pressures at the edges of the shell. Equating these two terms and dividing each side by dr, one gets

$$\frac{dP\left(r\right)}{dr} = \frac{dF}{4\pi r^2 dr} = -\frac{Gm\left(r\right)\rho\left(r\right)}{r^2}. \tag{3.1.2}$$

Using also the expression for $m(r)$

$$\frac{dm\left(r\right)}{dr} = 4\pi r^2 \rho\left(r\right), \tag{3.1.3}$$

we have now a closed set of two first order coupled differential equations that can be solved with some boundary conditions once we have a relation between pressure $P(r)$ and density $\rho(r)$. Here we want to point out that in Newtonian treatment the density stands for the pure mass density, while when we deal with General Relativity, due to the equivalence between mass and energy, $\rho(r)$ assumes the character of an energy density divided by c^2 , namely $\rho(r) = \mathcal{E}/c^2$.

As we said above, when studying neutron stars one as to take into account Einstein's theory of gravity: the parameter that gives an idea of the weight of general relativity corrections is compactness $C = R_s/R$. It is a dimensionless parameter defined by the ratio between the Schwarzschild radius ($R_s = 2GM/c^2$) and the radius of the star. The closer the compactness parameter of an object, such as a neutron star, is to 1, the stronger the effects of general relativity become, emphasizing the importance of considering General Relativity when describing such objects. In fact, a compactness parameter approaching 1 would indicate that the object is so dense that it may resemble a black hole, which cannot be accurately described by Newtonian mechanics

alone. In particular for neutron stars the compactness parameter goes around $0.2-0.4$ while for typical stars, for which a relativistic treatment is not necessary, is only of the order 10^{-6}.
We are now going to sketch a derivation of the hydrostatic equilibrium equations in General Relativity, the so called Tolman-Oppenheimer-Volkoff (TOV) equations following the original work did by Volkoff and Oppenheimer in 1939 [20], similar discussions can be found in [21] and [22]. The idea is to solve Eistein's field equations for a static, spherically symmetric spacetime in the presence of a non-zero energy-momentum tensor, since in our case there's some matter distribution unlike the simpler Schwarzschild solution for empty space. Let us consider first the most general static, spherically symmetric metric form

$$ds^2 = e^{-2\alpha(r)}dt^2 + e^{2\beta(r)}dr^2 + r^2 d\Omega^2. \tag{3.1.4}$$

From it one can compute the tensors to insert in Einstein equation

$$G_{\mu\nu} = R_{\mu\nu} - \frac{1}{2}Rg_{\mu\nu} = 8\pi G T_{\mu\nu}. \tag{3.1.5}$$

In the present model we are going to consider the matter distribution as a perfect fluid with energy-momentum tensor:

$$T_{\mu\nu} = (\rho + p)\, U_\mu U_\nu + p g_{\mu\nu}, \tag{3.1.6}$$

where the 4-velocity U_ν (that is has to be normalized to -1), since we are seeking static solutions, is taken to be pointing in the time-like direction:

$$U_\mu = (e^\alpha, 0, 0, 0)\,. \tag{3.1.7}$$

Since the energy-momentum tensor is diagonal, we have only three independent components of Einstein equation (we would have four but two of them are not independent), that are the one corresponding to tt, rr and $\theta\theta$ indices in the tensors above. It is now convenient to replace $e^{2\beta}$ with a new function that contains $m(r)$

$$e^{2\beta} = \left[1 - \frac{2Gm\,(r)}{r}\right]^{-1}. \tag{3.1.8}$$

The equation for tt term than becomes

$$\frac{dm}{dr} = 4\pi r^2 \frac{\mathcal{E}(r)}{c^2}. \tag{3.1.9}$$

It is interesting to notice one fact: integrating the energy density over the interior of the star (3.1.9) using the usual $dV = r^2 sin(\theta) dr d\theta d\phi$ (infinitesimal volume) in spherical coordinates one obtains a function $m(r)$ which can be interpreted as the mass within a radius r. Since we are dealing with a non-flat metric, though, the volume element should be $d\widetilde{V} = e^\beta dV$ instead. Hence, by integrating again, this time one gets another function $\widetilde{m}(r)$ which is the true integrated energy density. The difference between such two functions $\widetilde{m}(r) - m(r)$ corresponds to the gravitational binding energy. Combining the rr equation, with the one resulting from the energy-momentum conservation $\nabla_\mu T^{\mu\nu}$ (instead of using $\theta\theta$ term which would be more difficult), one eventually finds

$$\frac{dP\,(r)}{dr} = -\frac{G}{r^2}\left[\frac{\mathcal{E}\,(r)}{c^2} + \frac{P\,(r)}{c^2}\right]\left[m\,(r) + 4\pi r^3 \frac{P\,(r)}{c^2}\right]\left[1 - \frac{2Gm\,(r)}{c^2 r}\right]^{-1}, \tag{3.1.10}$$

that is the coveted Tolman-Oppenheimer-Volkoff equation with $\mathcal{E} = \rho c^2$ as we have already noted. The first two factor in squared brackets represent the special relativity corrections, and the third term comes from the general relativity.
Note how the TOV equation can be traced back to Newton's equation 3.1.2, in the limit of low compactness $(2Gm(r))/c^2 \ll r$, and velocities much less than the speed of light, such that $\mathcal{E}$ corresponds to the mass energy density alone and also $P(r)$ which, in the non-relativistic limit, goes like v^2 so that in the non-relativistic limit the term $P(r)/c^2$ is negligible. Similarly to the Newtonian case in order to solve the coupled system formed by (3.1.9) and (3.1.10), an equation of state $P = P(\mathcal{E})$ is needed. In their original work Tolman and Oppenheimer considered the equation of state of a non-interacting Fermi gas, that led them to a results of $0.7M_\odot$ for the maximum stable mass for neutron stars, the so called Tolmann-Oppenheimer-Volkoff limit, which the observations proved to be wrong. Indeed neutrons interact with each other resulting in a strong repulsive force and the effect is that the pressure generated in such a way can support more mass. This demonstrate how the EoS is such an important ingredient in the study of neutron stars, that's why the subject falls into the nuclear physics domain.

3.2 Tidal deformability

A tidal phenomenon can also be observed on Earth, high tide and low tide alternate twice every day, due to the gravitational interaction with the moon. Actually not only the sea undergo such a deformation, but also the entire Earth, even though in a less noticeable way. More in general, every time an object is subject to an external gravitational field which is not homogeneous, i.e., in presence of a non zero gradient of the gravitational field, that object undergoes a tidal deformation. The latter strongly depends on the structure and the matter of which the object is made of, that's why we'll be interested in the study of this topic. Under extreme conditions, for example in the proximity of a black hole where the gravitational field is incredibly strong the consequences of these tidal effects are terrific and produce one of the most spectacular events Nature is capable to create, the so called "tidal disruption events". The parameter that quantifies how easily an object deforms when subject to an external tidal field is the tidal deformability:

$$\lambda \equiv -\frac{Q_{ij}}{\mathcal{E}_{ij}} \tag{3.2.1}$$

where $\mathcal{E}_{ij}$ is a rank two tensor (3×3) matrix which in the Newtonian limit is defined as the second derivative of the gravitational field [23]

$$\mathcal{E}_{ij} = \frac{\partial^2 \Phi_{ext}}{\partial x^i \partial x^j}, \tag{3.2.2}$$

where $i, j = 1, 2, 3$ are spatial indexes. Q_{ij} is the quadrupole momentum response to the tidal field, which once again in Newtonian limit is

$$Q_{ij} = \int d^3x \delta\rho\,(x) \left(x_i x_j - \frac{1}{3} r^2 \delta_{ij} \right), \tag{3.2.3}$$

where $i, j = 1, 2, 3$ are spatial indexes, δ_{ij} is the Kronecker delta, $\delta\rho(r)$ is the mass density perturbation and x_i are the cartesian components. Q_{ij} is by definition a traceless tensor, i.e. such that $Q_{xx} + Q_{yy} + Q_{zz} = 0$, which quantifies the deviation of the mass distribution of a system from a spherically symmetric one.
The mass quadrupole is the counterpart of the electric charge quadrupole and following this analogy one can express the resulting gravitational potential as

$$V_q\left(\overrightarrow{R}\right) = -\frac{G}{2\left|\overrightarrow{R}\right|^3}\sum_{ij} Q_{ij}\widehat{R}_i\widehat{R}_j\,. \tag{3.2.4}$$

The third power of R at the denominator, tells us how the tidal contribution falls quickly and becomes less decisive away from the source. For instance, while the correction to the gravitational potential created by the Earth's tidal deformation is significant for artificial satellites, it becomes less relevant for more distant objects like the Moon. More details for the tidal field and the mass quadrupole consistent with general relativity can be found in [24].
Looking at Eq. 3.2.1 and also considering that $\mathcal{E}_{ij}$ has dimensions of an inverse length squared and Q_{ij} has dimensions of a length to the cube, overall we expect $\lambda \sim \kappa R^5$ where κ is a dimensionless term. Then tidal deformability is conventionally expressed as [23]:

$$\lambda = \frac{2}{3}k_2 R^5\,, \tag{3.2.5}$$

where k_2 is the tidal Love number. Love numbers are dimensionless parameters that measure the rigidity of a planetary body and the susceptibility of its shape to change in response to a tidal potential. The index 2 refers to the spherical harmonic of degree 2 of the tidal potential. In this work, as often in literature, the dimensionless tidal deformability Λ is used in place of λ:

$$\Lambda \equiv \frac{\lambda}{m^5} = \frac{64}{3}k_2 C^{-5}\,, \tag{3.2.6}$$

the compactness parameter $C = R_s/R$ is the one on which the dimensionless tidal deformability mostly depends.
Hinderer et. al. [25] provided calculations consistent with General Relativity (GR), also estimating that a Newtonian approach, that is the one in the above equations for tidal tensor and quadrupole tensor, brings an error around 20%.
The two tensors Q_{ij} and $\mathcal{E}_{ij}$ in the formalism of GR can be decomposed as:

$$\mathcal{E}_{ij} = \sum_{m=-2}^{2}\mathcal{E}_m\mathcal{Y}^{2m}_{ij}, \tag{3.2.7}$$

and

$$Q_{ij} = \sum_{m=-2}^{2}Q_m\mathcal{Y}^{2m}_{ij}, \tag{3.2.8}$$

where $\mathcal{Y}^{2m}_{ij}$ are symmetric traceless tensors defined by

$$Y_{2m}(\theta,\phi) = \mathcal{Y}^{2m}_{ij}n^i n^j\,, \tag{3.2.9}$$

with $\mathbf{n}$ =(sinθcosϕ,sinθsinϕ, cosθ).
The results are obtained by Hinderer following the previous findings of Thorne &

Campolattaro [26], in the star's local asymptotic rest frame the metric element g_{tt} is defined by

$$\begin{aligned}\frac{(1-g_{tt})}{2} = -\frac{M}{r} - \frac{3Q_{ij}}{2r^3}\left(n^i n^j - \frac{1}{3}\delta^{ij}\right) + \\ +O\left(\frac{1}{r^3}\right) + \frac{1}{2}\mathcal{E}_{ij}x^i x^j + O\left(r^3\right) \,,\end{aligned} \tag{3.2.10}$$

where $n_i = x_i/r$. By imposing continuity of the metric and its derivatives across the border of the neutron star and treating the quadrupolar tidal field as a perturbation, they get an expression of k_2 which depends on the star's compactness parameter and a function $y(r)$, that is implicitly defined by the expression

$$r\frac{dy(r)}{dr} + y^2(r) + y(r)F(r) + r^2 Q(r) = 0\,, \tag{3.2.11}$$

as pointed out in [27] where

$$F(r) = \left[1 - \frac{4\pi r^2 G}{c^4}\left(\mathcal{E}(r) - P(r)\right)\right]\left(1 - \frac{2M(r)G}{rc^2}\right)^{-1} \tag{3.2.12}$$

and,

$$\begin{aligned}r^2 Q(r) = \frac{4\pi r^2 G}{c^4}\left[5\mathcal{E}(r) + 9P(r) + \left(\frac{\mathcal{E}(r)+P(r)}{\partial P(r)/\partial\mathcal{E}(r)}\right)\right]\left(1-\frac{2M(r)G}{rc^2}\right)^{-1} + \\ -6\left(1-\frac{2M(r)G}{rc^2}\right)^{-1} + \\ -\frac{4M^2(r)G^2}{r^2c^4}\left(1+\frac{4\pi r^3 P(r)}{M(r)c^2}\right)^2\left(1-\frac{2M(r)G}{rc^2}\right)^{-2}.\end{aligned} \tag{3.2.13}$$

By numerical integration of the expression of 3.2.11 together with the TOV equation, considering also $y(0) = 2$ [25] one can find the value of $y_R = y(R)$, where R is the radius of the star. Finally using y_R along with the values of mass and radius of the star (or the compactness parameter) one can compute k_2 as follows:

$$\begin{aligned}k_2 = \frac{1}{20}C^5(1-C)^2\left[2 - y_R + (y_R-1)C\right] \\ \times\Bigg\{C\Bigg(6 - 3y_R + \frac{3}{2}C(5y_R-8) + \frac{1}{4}C^2 \\ \times\left[26 - 22y_R + C(3y_R-2) + C^2(1+y_R)\right]\Bigg) \\ +3(1-C)^2\left[2-y_R+(y_R-1)C\right]\ln(1-C)\Bigg\} - 1.\end{aligned} \tag{3.2.14}$$

It can also be noted that also the rotation of the star contributes to a quadrupole deformation but this additional effect is not considered in the present work, since we focused on static neutron stars.

3.2.1 Estimating neutron star's properties from Gravitational Waves

In 2017 the first detection of gravitational waves (GW) predicted by Einstein's theory of General Relativity started the new age of multi-messenger astrophysics. In a binary system, i.e., a system of two orbiting compact objects (black holes, neutron stars...) in a spiral motion that are doomed to collide with each other. During the period of coalescence a great amount of energy is dissipated in the form of gravitational waves, in analogy with an accelerated electric charge which emits electromagnetic waves. Let us consider now a binary system of two neutron stars: as we have already explained above, each neutron star will be subject to the tidal field of its companion, so it deforms in a quadrupolar mode (Fig.3.2) and the time scale of this deformation is faster than the orbital motion that modulates the tidal field, so the two bulges of neutron stars will always face each other [23].

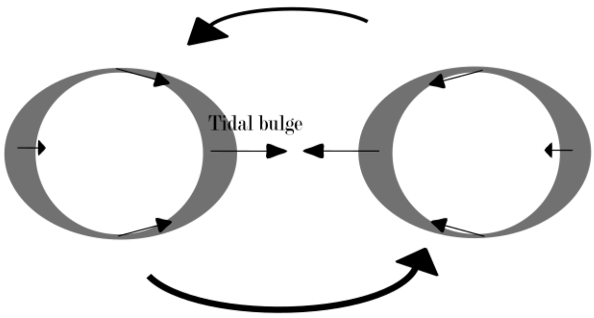

Figure 3.2: Scheme of a binary system in which neutron stars undergo a tidal deformation due to companion's gravitational field.

Tidal effects affect both the amplitude and the phase of the gravitational wave signal. To give an idea of how masses and tidal deformabilities are extracted from the wave signal let us consider the expression of the GW phase:

$$\begin{aligned} \psi\left(f\right) = 2\pi f t_c + \phi_c - \frac{\pi}{4} + \\ + \frac{3}{128\eta u^5}\left\{1 + f\left(\eta\right)u^2 + \left(4\beta - 16\pi\right)u^3 + \left[g\left(\eta\right) + \sigma\right]u^4 + , \\ + \ldots - \frac{39}{2}\widetilde{\Lambda}u^{10} + \ldots\right\} \end{aligned} \tag{3.2.15}$$

for which the computation is performed in a post-Newtonian fashion, i.e. an approach in which the effects of General Relativity are embedded as corrections in Newtonian theory, by means of an expansion in terms of the metric tensor and small binary velocity u (in units of c).
In 3.2.15 f is the frequency of the GW, t_c and Φ_c are the time and the phase of coalescence respectively, $u = (\pi M f)^{1/3}$, $M = M_1 + M_2$ is the total mass. The functions $f(\eta)$ and $g(\eta)$ can be found, for example in [28], while the terms β and σ represent spin-orbit and spin-spin contributions to the phase respectively. For a more exhaustive discussion of all the terms see [28; 27].
For the purposes of this work, we'll just emphasize the fact that the only terms that can be directly inferred from the study of GW signal are:

$$\mathcal{M} = M\eta^{3/5} \tag{3.2.16}$$

where η is the reduced mass, and

$$\widetilde{\Lambda} = \frac{16}{3}\frac{(m_1 + 12m_2)\, m_1^4\Lambda_1 + (m_2 + 12m_1)\, m_2^4\Lambda_2}{(m_1 + m_2)^5}\,, \tag{3.2.17}$$

respectively the chirp mass and a combination of the single dimensionless tidal deformabilities. In order to get single masses and tidal deformabilities to compare to our model, more sophisticated work has to be done. Neutron star masses can be independently constrained from the lower orders in the post-Newtonian expansion of the waveform phase, while the single tidal deformabilities can be inferred from $\widetilde{\Lambda}$ studing some "EoS insensitive" relations, i.e looking for some properties that are weakly depending on the EoS adopted in the model, for example noticing the $\tilde{m}^{-5}$ dependence of Λ: more details are given in [29].

3.3 Building the equation of state: from a macroscopical point of view to mean field theories

As previously stated, in order to form a closed system, i.e. a system that can be solved, TOV equation must be complemented by an "Equation of State" (EoS), which establishes a relation between the energy density and pressure. The EoS is determined by the model for nuclear matter that we choose to implement. It should be noted that different models may yield different EoSs, and there are still uncertainties regarding the behavior of nuclear matter under extreme conditions.

In our model we'll consider neutron stars as bound systems of protons, neutrons, electrons and muons, not including other exotic particles,such as the hyperons, for the reasons explained in Chapter 2.

Neutron stars are characterized by extreme conditions that allow neutrons to form a bound system through the force of gravity. In contrast, a highly neutron-rich configuration is not stable under normal density conditions, as in laboratories on earth. This is due to the fact that free neutrons are unstable, indeed they decay beta in protons, electrons and neutrinos.

Despite their name, neutrons stars cannot be made only of neutrons. To meet the requirements of beta-equilibrium and charge neutrality, a certain proportion of protons and electrons are necessary. Chapter 4 provides a detailed discussion of this topic. In the latter is also explained the appearance of muons and in particular a method to compute threshold density value starting from which muons are energetically favorable.

The best thermodynamic potential to study our system is the internal energy. More precisely when dealing with an idealized system of infinite nuclear matter, such as the one we have considered in our calculation, it is better to work with energy densities instead of energies. This is the first block needed to build an equation of state. It is useful to divide the contributions to the total energy density into nuclear, electronic, and muonic:

$$\mathcal{E} = m_n n_n c^2 + m_p n_p c^2 + \mathcal{E}_{nucl} + \mathcal{E}_{elec} + \mathcal{E}_{\mu}. \tag{3.3.1}$$

The first two terms in the expression represent the rest mass energies of neutrons and protons, the third term is the energy coming from the interaction between nucleons and the last two terms are the electrons and muons contributions respectively. We focus in particular on the third term, investigating some of the most widely used models that describe nuclear interactions. At the end of this section we also describe how electron and muons contributions enter in the total energy formula.

3.3.1 A first crude nuclear model

To provide an idea of how modern models for nuclear matter have been developed and a justification for the need for microscopic theories, this section briefly illustrates the first model used to describe the properties of atomic nuclei, namely the one of Bethe and Weizsäcker (BW). This model will not be implemented in our calculations since it does not consider the contribution of nuclei to pressure and hence cannot provide a counterpart to the extreme gravity in neutron stars.
Bethe and Weizsäcker (BW), in 1935 [30] proposed a formula for the binding energy of a system composed by a number A of nucleons. The mass of such a system is given by

$$M = Zm_p + Nm_n - E_B/c^2\,, \tag{3.3.2}$$

where Z is the number of protons, N the number of neutrons and the last term has just the units of a mass, according to Eistein's theory of Special Relativity which states the equivalence of mass and energy. The binding energy E_B is given by BW formula:

$$E_B = a_V A - a_S A^{2/3} - a_C \frac{Z(Z-1)}{A^{1/3}} - a_A \frac{(N-Z)^2}{A} + \delta(N,Z)\,, \tag{3.3.3}$$

which describes nuclei as liquid drops. Different methods for fitting the coefficients a_i have been implemented. For instance using least squares method typical values are $a_v = 15.8MeV$, $a_s = 18.3MeV$, $a_c = 0.714MeV$, $a_a = 23.2MeV$, and $\delta = \pm 12/\sqrt{A}MeV$. Slightly different values found using other fitting methods are available in [31; 32]. The first term is the dominant and it's known as "volume term", it quantifies the strong nuclear force between nucleons, which is a short-range force and then proportional to the number of neighbors each nucleon has. Since $R = r_0 A^{1/3}$, this term is eventually proportional to the volume. The second term is once again related to the strong interaction but this time is subtractive, it reflects the fact that nucleons on the surface have fewer neighbors, it is called "surface term" since it is proportional to the surface ($A^{2/3}$) of the nucleus. The third term is the Coulomb term which describes the electric repulsion between protons which is not difficult to calculate if a uniformly charged sphere is assumed.
The last two terms are the asymmetry energy and the pairing energy respectively: the former accounts for the Pauli exclusion principle and can be understood as the energy required to transform a proton into a neutron and vice versa departing from a symmetrical distribution. Being both fermions, at most two identical particles can occupy the same energy level (with opposite spin), for example converting a proton into a neutron, starting from a condition in which the uppermost energy level is filled, requires the new neutron to go to the first unoccupied energy level above the last occupied one. The new system has now an higher total energy, so it's less bound (see Fig. 3.3 for a pictorial representation of the argument).
By definition Bethe and Weizsäcker's formula is quite good in predicting the mass of nuclei with A$\geq$ 50 with an accuracy in the range $[0.5\%, 1.5\%]$ [33] , but fails when other nuclear properties such as excited states are taken into exam. That's why other

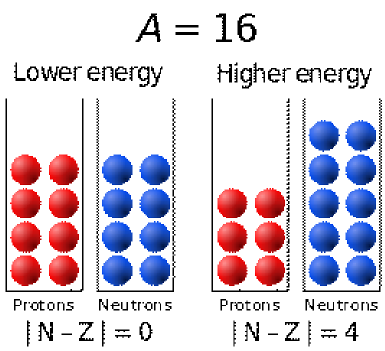

Figure 3.3: Visualizing the asymmetry term in Bethe-Weizsäcker formula.

approaches over the years have been developed, as new nuclear properties have been observed in laboratories with which a candidate nuclear model shall be in accordance, these models lead us to a microscopical description.

3.3.2 Mean-field theories: Skyrme-type interactions

When dealing with a many-body system, determining and predicting its behavior can be quite complicated. Solving a Hamiltonian that describes all the interactions between each particle becomes unfeasible as the number of particles increases. In fact, even for an atom with many electrons, a non-trivial approach is needed, such as using Slater determinants and Hartree-Fock calculations. The mean-field approach is an approximation used to understand the behavior of interacting systems. It assumes that each particle only experiences the average action of all the other particles, allowing for a simplified analysis of the system but still quite accurate.
A first model, a widely used one, is that originally proposed by T. H. R. Skyrme in 1956 [34] which assumes zero-range forces for interactions between particles resulting in quite simple analytical calculations. Indeed, all the terms in it are proportional to Dirac deltas which can be easily treated. Skyrme-type interactions follows the same structure expressed by the potential

$$\begin{aligned} V_{SKY}\left(\boldsymbol{r}_1, \boldsymbol{r}_2\right) = {} & t_0\left(1+x_0 P_\sigma\right) \delta\left(\boldsymbol{r}_1-\boldsymbol{r}_2\right) \\ & +\frac{1}{2} t_1\left(1+x_1 P_\sigma\right)\left[\boldsymbol{k}'^2 \delta\left(\boldsymbol{r}_1-\boldsymbol{r}_2\right)+\delta\left(\boldsymbol{r}_1-\boldsymbol{r}_2\right) \boldsymbol{k}'^2\right] \\ & +t_2\left(1+x_2 P_\sigma\right)\left[\boldsymbol{k}' \cdot \delta\left(\boldsymbol{r}_1-\boldsymbol{r}_2\right) \boldsymbol{k}\right] \\ & +\frac{1}{6} t_3\left(1+X_3 P_\sigma\right)[n(\boldsymbol{R})]^\sigma \delta\left(\boldsymbol{r}_1-\boldsymbol{r}_2\right) \\ & +i W_0 \overrightarrow{\sigma}\left[\boldsymbol{k}' \times \delta\left(\boldsymbol{r}_1-\boldsymbol{r}_2\right) \boldsymbol{k}\right], \end{aligned} \tag{3.3.4}$$

where $t0, t1, t2, t3, x0, x1, x2, x3, W_0, \sigma$ are parameters that identify one particular Skyrme parametrization. Other quantities are defined as

$$R=\frac{1}{2}\left(\boldsymbol{r}_1+\boldsymbol{r}_2\right), \tag{3.3.5}$$

$$\boldsymbol{k} = \frac{1}{2i}\left(\overrightarrow{\nabla}_1 - \overrightarrow{\nabla}_2\right) , \tag{3.3.6}$$

$$\boldsymbol{k'} = \frac{1}{2i}\left(\overleftarrow{\nabla}_2 - \overleftarrow{\nabla}_1\right) , \tag{3.3.7}$$

$$\overrightarrow{\sigma} = \overrightarrow{\sigma}_1 + \overrightarrow{\sigma}_2 , \tag{3.3.8}$$

$$P_\sigma = \frac{1 + \overrightarrow{\sigma}_1 \cdot \overrightarrow{\sigma}_2}{2} . \tag{3.3.9}$$

The first term in 3.3.4 is a central force term which depends only on positions (i.e. is local), the second and the third term contain momenta dependence hence are not local, the fourth term simulate a three-body interaction $V_{123} = t_3\delta\left(\boldsymbol{r}_1 - \boldsymbol{r}_2\right)\delta\left(\boldsymbol{r}_2 - \boldsymbol{r}_3\right)$by means of a two-body density-dependent interaction $n(\boldsymbol{R})$: this term provides a phenomenological representation of many-body effects. Finally the fifth term represents spin-orbit interaction.

Skyrme parameters are found with fitting procedures with the available data on nuclei, the distinction from one to another is given by the different choices one can take, regarding the weights to give to the observables with which the model is fitted. A great number of different Skyrme parametrizations have been implemented in the study of neutron stars, for a review of the most famous see [35]. Just to give an example, the two first parametrizations were found by Vautherin and Brink [36] in 1972, which makes good predictions for binding energies and radii for ^{16}O and ^{208}Pb, and all closed shell nuclei, they are also in good qualitatively agreement with electron scattering angular distributions.

All the procedures take into account in the first place the the available data on binding energy and the mass of some nuclei, other pseudo-observable which are investigated can be the saturation density, the effective mass of nucleons and its momentum dependence [37], the incompressibility K [38] , the symmetry energy and its density dependence [39], the skewness [40] and others.

It should be noted that Skyrme-type parametrizations have been built for densities similar to those found in nuclei studied on Earth. However, when it comes to extreme density conditions in neutron stars, the effectiveness of these models is no longer certain. What can be done is to extrapolate the models to higher densities, such as those found in the description of neutron stars, and evaluate the accuracy of the predictions against observed parameters.

The calculation are Hartree-Fock type, for which once an Hamiltonian H and a general many-particles wave function $|\phi>$, in the form of Slater determinant, are taken, performing a variation of the mean value of H in the state $|\phi>$, i.e. the energy of the system, by varying the single-particle wave functions in an iterating process one gets finally the best approximated expressions of the wave functions ϕ_i .

The mean energy of a system composed of a certain number of nucleons, considering the wave function of the system as a Slater determinant, is given by the standard computation:

$$\begin{aligned} <\Phi\left|H\right|\Phi> &= \sum_i < \phi_i \left|\frac{p_i^2}{2m_i}\right|\phi_i> + \frac{1}{2}\sum_{ij} < \phi_i\phi_j|\overline{V}_{SKY}|\phi_i\phi_j> \\ &= \int d^3r\mathcal{H}\left(r\right) , \end{aligned} \tag{3.3.10}$$

where the first term represent the mean kinetic energy which, supposing the system in its ground state is the same as for a Fermi gas, i.e. momentum p corresponds to the

Fermi momentum p_F. The second term is the one regarding the two body interaction between nucleons where $\overline{V}_{SKY}$ denotes an antisymmetrized matrix element. The latter characteristic is due to the form of the Slater determinant, which by definition is a completely antisymmetric combination of single-particle wave functions.
We denote $\mathcal{H}(r)$ as the energy functional. Reminding now, the expression for Skyrme potential in eq. 3.3.4 and entering it in eq. 3.3.10 after some calculations [36] one gets to the complete Skyrme functional, which has the units of an energy density

$$\mathcal{H} = \mathcal{K} + \mathcal{H}_0 + \mathcal{H}_3 + \mathcal{H}_{eff} + \mathcal{H}_{fin} + \mathcal{H}_{SO} + \mathcal{H}_{sg}\,, \tag{3.3.11}$$

where

$$\mathcal{K} = \frac{3}{5} n_n E_{F,n} + \frac{3}{5} n_p E_{F,p}\,, \tag{3.3.12}$$

is the kinetic energy depending on Fermi energies of both neutrons and protons

$$E_{F,i} = \frac{\hbar^2}{2m_i}(3\pi^2 n_i)^{2/3}\,,$$

$$\mathcal{H}_0 = \frac{1}{4} t_0 \left[(2 + x_0)\, n^2 - (2x_0 + 1)\left(n_n^2 + n_p^2\right)\right] \tag{3.3.13}$$

is a zero-range term,

$$\mathcal{H}_3 = \frac{1}{24} t_3 n^\sigma \left[(2 + x_3)\, n^2 - (2x_3 + 1)\left(n_n^2 + n_p^2\right)\right] \tag{3.3.14}$$

is the density dependent term,

$$\begin{aligned}\mathcal{H}_{eff} = &\frac{1}{8}\left[t_1 (2 + x_1) + t_2 (2 + x_2)\right] \tau n + \\ &+ \frac{1}{8}\left[t_2 (2x_2 + 1) - t_1 (2x_1 + 1)\right] (\tau_n n_n + \tau_p n_p)\end{aligned} \tag{3.3.15}$$

is an effective mass term,

$$\begin{aligned}\mathcal{H}_{fin} = &\frac{1}{32}\left[3t_1 (2 + x_1) - t_2 (2 + x_2)\right]\left(\overrightarrow{\nabla} n\right)^2 + \\ &- \frac{1}{32}\left[3t_1 (2x_1 + 1) + t_2 (2x_2 + 1)\right] \cdot \left[\left(\overrightarrow{\nabla} n_n\right)^2 + \left(\overrightarrow{\nabla} n_p\right)^2\right]\end{aligned} \tag{3.3.16}$$

is a finite range term,

$$\mathcal{H}_{so} = -\frac{1}{2} W_0 \left[\boldsymbol{J} \cdot \overrightarrow{\nabla} n + \boldsymbol{J}_n \cdot \overrightarrow{\nabla} n_n + \boldsymbol{J}_p \cdot \overrightarrow{\nabla} n_p\right] \tag{3.3.17}$$

is a spin-orbit term and

$$\begin{aligned}\mathcal{H}_{sg} = &\frac{1}{16} t_1 \left(\boldsymbol{J}_n^2 + \boldsymbol{J}_p^2 - x_1 \boldsymbol{J}^2\right) + \\ &- \frac{1}{16} t_2 \left(\boldsymbol{J}_n^2 + \boldsymbol{J}_p^2 + x_2 \boldsymbol{J}^2\right)\end{aligned} \tag{3.3.18}$$

is a term representing the coupling with spin and gradient. In the equations above, n_i are the particle number densities, $\tau_i = (3/5)k_{F,i}^2$ where k_F is the Fermi constant are the kinetic energy densities, and

$$\boldsymbol{J}_q(\boldsymbol{r}) = -i \sum_{i,s,s'} (\phi_i^q)^*(\boldsymbol{r}, s')\overrightarrow{\nabla}\phi_i^q(\boldsymbol{r}, s) \times \langle s'|\overrightarrow{\sigma}|s\rangle \tag{3.3.19}$$

is the spin-orbit density term where q is an isospin index ($q = 1/2$ for protons and $q = -1/2$ for neutrons). The other quantities with no index are defined as

$$\begin{aligned} n &= n_p + n_n \,, \\ \tau &= \tau_n + \tau_p \,, \\ \boldsymbol{J} &= \boldsymbol{J}_n + \boldsymbol{J}_p \,. \end{aligned} \tag{3.3.20}$$

The definition of an energy functional allows one to compute the total energy per baryon, the latter to be discussed in next section.

3.3.3 Infinite nuclear matter: energy density and pressure for Skyrme type interactions

In the present work we have considered an infinite nuclear matter model, a system with protons and neutrons with no Coulomb interactions. Such an hypothesis rules out some of the terms in 3.3.11. Indeed, infinite nuclear matter in ground state has $\boldsymbol{J} = 0$ since an equal number of particles with spin up and spin down are present, namely a spin saturated system. Furthermore, we assumed (at least locally) uniform matter, resulting in $\overrightarrow{\nabla} n_i = 0$.
We are left with only the first four terms of eq. 3.3.11.
Computing the energy per nucleon is now a trivial task:

$$\frac{E}{A} = \frac{\mathcal{H}}{n} \,. \tag{3.3.21}$$

A first requirement for a particular choice of Skyrme parameters, is the value of E/A for symmetric nuclear matter SNM (equal number of protons and neutrons) that at the **saturation density** n_0 must be minimized.
The value of $E/A(n_0)$ can be determined via the liquid drop model described in section 3.3.1, in particular it corresponds to the term a_V in the formula 3.3.3 which is equal to $-16 \pm 0.2\ MeV$. Neutron stars are made not only of neutrons as described in previous chapters, but also of protons, electrons and other more exotic particles, is than useful to display the results for the more general case of asymmetric infinite nuclear matter.
Instead of writing down an expression for E/A depending on n_n and n_p let's introduce a parameter which describes the neutron aboundance:

$$\delta \equiv \frac{n_n - n_p}{n_n + n_p} = \frac{n_n - n_p}{n} \,, \tag{3.3.22}$$

substituting the general expression 3.3.11 into 3.3.21 and also taking into account parameter δ just defined one gets

$$\begin{aligned}\frac{E}{A}(n,\delta) = &\frac{3}{10}\frac{\hbar^2}{2m_N}\left(\frac{3\pi^2}{2}\right)^{2/3}\left[(1-\delta)^{5/3}+(1+\delta)^{5/3}\right]n^{2/3}\\ &+\frac{1}{4}t_0 n\left[2+x_0-\frac{2x_0+1}{2}\left(1+\delta^2\right)\right]\\ &+\frac{1}{24}t_3 n^{\sigma+1}\left[2+x_3-\frac{2x_3+1}{2}\left(1+\delta^2\right)\right]\\ &+\frac{3}{80}\left(\frac{3\pi^2}{2}\right)^{2/3}\left[t_1\left(2+x_1\right)+t_2\left(2+x_2\right)\right]\left[(1-\delta)^{5/3}+(1+\delta)^{5/3}\right]n^{5/3}\\ &+\frac{3}{160}\left(\frac{3\pi^2}{2}\right)\left[t_2(2x_2+1)-t_1(2x_1+1)\right]^{2/3}\left[(1-\delta)^{5/3}+(1+\delta)^{5/3}\right]n^{5/3}.\end{aligned} \tag{3.3.23}$$

The following expression for symmetric nuclear matter ($\delta = 0$) is than straightforward:

$$\begin{aligned}\frac{E}{A}(n,\delta=0) = &\frac{3}{5}\frac{\hbar^2}{2m_N}\left(\frac{3\pi^2}{2}\right)^{2/3}n^{2/3}\\ &+\frac{3}{8}t_0 n+\frac{1}{16}t_3 n^{\sigma+1}\\ &+\frac{3}{80}\left(\frac{3\pi^2}{2}\right)^{2/3}\left[3t_1+t_2\left(5+4x_2\right)\right]n^{5/3}.\end{aligned} \tag{3.3.24}$$

The total energy per nucleon as given in Eq. 3.3.23 can be expanded around $\delta = 0$ recalling the Taylor expansion of the kind:

$$(1+\delta)^{\alpha} = 1+\alpha\delta+\alpha(\alpha-1)\delta^2+O(\delta^3) \tag{3.3.25}$$

the results is the following:

$$\frac{E}{A}(n,\delta) = \frac{E}{A}(n,\delta=0)+E_{sym}\delta^2+... \tag{3.3.26}$$

with

$$\begin{aligned}E_{sym}(n) = &\frac{1}{3}\frac{\hbar^2}{2m_N}\left(\frac{3\pi^2}{2}\right)^{2/3}n^{2/3}\\ &-\frac{1}{8}t_0 n(2x_0+1)-\frac{1}{48}t_3 n^{\sigma+1}(2x_3+1)\\ &+\frac{1}{24}\left(\frac{3\pi^2}{2}\right)^{2/3}\left[t_2\left(4+5x_2\right)-3t_1x_1\right]n^{5/3},\end{aligned} \tag{3.3.27}$$

where we have defined the **symmetry energy** E_{sym} as the coefficient of δ^2 in the Taylor expansion. It may be noticed that due to expansion of terms in couple as $(1-\delta)^{\alpha}+(1+\delta)^{\alpha}$ the odd terms cancel out, the physical meaning is that there is no energy difference in converting one proton into a neutron and viceversa, this is due to the isospin symmetry. The term "symmetry energy" comes from the fact that it represents a second order correction to the system's energy associated with isospin symmetry. Several articles (see for instance [41]) showed a detailed calculation of E/A demonstrating how higher order terms in 3.3.26 are basically negligible not only near $\delta = 0$. Nevertheless in this work the complete solution 3.3.23 is always adopted in our computations.

The symmetry energy is usually expanded around the saturation density n_0 (see e.g ref [42])

$$E_{sym} \approx J + L\frac{n - n_0}{3n_0} + \frac{K_{sym}}{2}\frac{(n - n_0)^2}{(3n_0)^2} + \mathcal{O}(n - n_0)^3 \,, \tag{3.3.28}$$

which helps identifying useful parameters: J is the symmetry energy at saturation density, L is referred to as the slope parameter, i.e., the slope of the symmetry energy at saturation

$$L = 3n_0 \left(\frac{\partial E_{sym}(n)}{\partial n}\right)\bigg|_{n=n_0} . \tag{3.3.29}$$

Furthermore, at n_0 L is the slope not only of the symmetry energy but also of the total energy 3.3.26. Indeed the first term of the expansion 3.3.26, namely the energy of symmetric nuclear matter, has a minimum at n_0 and therefore its slope is zero at that point.

Finally the nuclear compressibility modulus is defined as

$$K_{sym} = 9n_0^2 \left(\frac{\partial^2 E_{sym}(n)}{\partial n^2}\right)\bigg|_{n=n_0} . \tag{3.3.30}$$

It represents the rigidity of the nucleus, that is, the resistance it opposes to a variation of its shape.

Many studies that used a variety of phenomenological and theoretical models or laboratory data to extract constraints on the density dependence of the symmetry energy (some references are given in [42]).

From the first law of thermodynamics, as in a neutron star the temperature is far less than Fermi temperature ($kT \ll E_F$), it's safe to say that the temperature is zero everywhere so also the entropy is zero. Hence pressure takes the form

$$P \equiv -\frac{\partial(E/A)}{\partial(1/n)} = n^2\frac{\partial(E/A)}{\partial n} \,, \tag{3.3.31}$$

where $1/n$ is the volume per baryon.

Inserting 3.3.23 into the previous equation 3.3.31, one gets the formula for pressure:

$$\begin{aligned} P_{nuc}\left(n,\delta\right) = &\frac{1}{5}\frac{\hbar^2}{2m_N}\left(\frac{3\pi^2}{2}\right)^{2/3}\left[(1-\delta)^{5/3} + (1+\delta)^{5/3}\right]n^{5/3} \\ &+ \frac{1}{4}t_0 n^2\left[2 + x_0 - \frac{2x_0+1}{2}\left(1+\delta^2\right)\right] \\ &+ \frac{1}{24}(\sigma+1)t_3 n^{\sigma+2}\left[2 + x_3 - \frac{2x_3+1}{2}\left(1+\delta^2\right)\right] \\ &+ \frac{1}{16}\left(\frac{3\pi^2}{2}\right)^{2/3}\left[t_1\left(2+x_1\right) + t_2\left(2+x_2\right)\right]\left[(1-\delta)^{5/3} + (1+\delta)^{5/3}\right]n^{8/3} \\ &+ \frac{1}{32}\left(\frac{3\pi^2}{2}\right)\left[t_2(2x_2+1) - t_1(2x_1+1)\right]^{2/3}\left[(1-\delta)^{5/3} + (1+\delta)^{5/3}\right]n^{8/3}. \end{aligned} \tag{3.3.32}$$

From the energy density ($\mathcal{E}_{nuc} = nE/A$) and from pressure (Eq. 3.3.32) is now possible to build the first part of the EoS, the one regarding the nuclear interactions. In order to get the complete EoS also muons and electrons contributions must be taken into account, the latter will be discussed next in this Chapter.

3.3.4 Mean field theories: Fayans functional

In 1998 S.A. Fayans proposed another totally different EDF (Energy density functional), [43] his work was an attempt toward a universal functional, capable to describe not also matter in nuclei but even matter at much higher densities ($\sim 1\,fm^{-3}$) as in neutron stars. Fayans pointed out the fact that models based on Skyrme type interactions, give results with rms deviations from experiment no better than about $2\,MeV$ and $0.02\,fm$ for masses and radii respectively, the relative error for radii is 4 times worse than the one for masses. He also suggested that a good EDF should have relative errors on masses and radii consistent with each other (of the same order).
In Fayans model the total energy density is written as:

$$\mathcal{E} = \mathcal{E}_{kin} + \mathcal{E}_v + \mathcal{E}_s + \mathcal{E}_{Coul} + \mathcal{E}_{sl} + \mathcal{E}_{anom} \,, \tag{3.3.33}$$

where the kinetic energy term is the same as in Skyrme case, while the volume term is:

$$\varepsilon_v = \frac{2}{3} E_{F,0} n_0 \left[a_+^v \frac{1 - h_{1+}^v x_+^\sigma}{1 + h_{2+}^v x_+^\sigma} x_+^2 + a_-^v \frac{1 - h_{1-}^v x_+}{1 + h_{2-}^v x_+} x_-^2 \right] . \tag{3.3.34}$$

Here $x_\pm = (n_n \pm n_p)/2n_0$, $E_{F,0} = (9\pi/8)^{2/3}\hbar^2/2mr_0^2$ with radius parameter $r = (3\pi n_0/8)^{1/3}$ and $2n_0 = 0.16\,fm^{-3}$ is the saturation density, such an expression gives an EoS that preserves causality (speed of sound is less than speed of light) even at high densities, while the 4 dimensionless parameters are fitted to UV14+TNI model of Friedman-Pandharipande and Wiringa-Fiks-Fabroncini [44; 45], they are $a_+^v = -9.559$, $h_{1+}^v = 0.633$, $h_{2+}^v = 0.131$, $a_-^v = 4.428$, $h_{1-}^v = 0.250$, $h_{2-}^v = 1.300$ and $\sigma = 1/3$.
In the hypothesis of infinite and homogeneous nuclear matter as the one considered in this work to studying neutron stars, all the other terms in Eq. 3.3.33 are taken to be zero, for the following reasons:
the surface term $\mathcal{E}_s$ and spin-orbit $\mathcal{E}_{sl}$ term depend on density variations, but density is constant, pairing term $\mathcal{E}_{anom}$ is zero because in infinite matter all the spin states (spin up and spin down) are filled and finally Coulomb term $\mathcal{E}_{Coul}$ is not accounted for, since in infinite matter it would diverge.
Following the same procedure as for Skyrme EDF, pressure can now be computed

using 3.3.31:

$$\begin{aligned}P_{fay}(n,\delta) = &\frac{1}{5}\frac{\hbar^2}{2m_N}\left(\frac{3\pi^2}{2}\right)^{2/3}\left[(1-\delta)^{5/3}+(1+\delta)^{5/3}\right]n^{5/3}\\ &+\frac{1}{3}E_{F,0}\frac{n^2}{2n_0}\left\{\left[a_+^v\frac{1-h_{1+}^v x_+^{1/3}}{1+h_{2+}^v x_+^{1/3}}+a_-^v\frac{1-h_{1-}^v x_+}{1+h_{2-}^v x_+}\delta^2\right]\right.\\ &\left.-n\cdot\left[a_+^v\frac{x_+^{-2/3}(1/6n_0)\left[h_{1+}^\nu+h_{2+}^\nu\right]}{\left(1+h_{2+}^v x_+^{1/3}\right)^2}+a_-^v\frac{\delta^2(1/2n_0)\left(h_{1-}^v+h_{2-}^v\right)}{\left(1+h_{2-}^v x_+\right)^2}\right]\right\}.\end{aligned} \tag{3.3.35}$$

Using the results 3.3.33 and 3.3.35 a different EoS can be built, the other pieces entering the EoS as muons and electrons contributions, and the merging with BPS EoS are just the same as in the Skyrme model.

3.3.5 Electrons and muons contributions

The electronic and muonic contributions are computed in the frame of a Fermi gas, as discussed in other sections the presence of electrons is called for in order to have a zero net charge neutron star and muons comes into play at higher densities when is energetically more convenient to produce them than further increasing the kinetic energy of electrons (further details in Chapter 4). First consider electrons contribution:
it can be demostrated that at high densities electron-electron interactions are negligible with respect to their Fermi energy [46], so are electron-nucleons interactions.
In a neutron star electrons are always considered to be ultrarelativistic, indeed it can be easily computed that kinetic energy becomes comparable to the rest mass starting from densities of the order $10^6 g/cm^{-3}$, several orders below the saturation density.
From special relativity we know that

$$E = (m_e^2 c^2 + p_{F,e}^2 c^2)^{1/2}\,, \tag{3.3.36}$$

where $p_{F,e}$ is Fermi momentum and corresponds to:

$$p_{F,e} = \hbar\left(3\pi^2 n_e\right)^{1/3}. \tag{3.3.37}$$

In the ultra-relativistic case the mass term in the energy is negligible, hence the energy density is given by:

$$\mathcal{E}_{elec} = \frac{8\pi}{h^3}\int_0^{+\infty} f(E)E4\pi p^2 dp\,, \tag{3.3.38}$$

where it has been used the infinitesimal volume in momentum space $d^3k = 4\pi k^2 dk$, an additional factor 2 is due to the giromagnetic factor for the electron and $f(E)$ is the Fermi-Dirac distribution which in the limit $T = 0$ reduces to:

$$f(E) = \begin{cases} 1 & E \leq E_F \\ 0 & E > E_F. \end{cases} \tag{3.3.39}$$

Inserting expressions 3.3.36 and 3.3.37 in the integral 3.3.38 the computation is straightforward:

$$\mathcal{E}_{elec} = \frac{\hbar c}{4\pi^2}(3\pi^2 n_e)^{4/3}\,. \tag{3.3.40}$$

Finally using the formula 3.3.31 and performing simple derivatives one gets:

$$P_{elec} = \frac{1}{3}\mathcal{E}_{elec}. \tag{3.3.41}$$

Similar calculations can be performed for the case of muons, although on the contrary are mild-relativistic instead ultra-relativistic. As a consequence one must take into account the entire expression 3.3.36 and performing the same integral 3.3.38 and derivation for pressure, this time a bit more difficult, the results comes out as follow [47]:

$$\mathcal{E}_\mu = \frac{m_\mu c^2}{\lambda_\mu^3}\left\{\frac{1}{8\pi^2}\left[x(1+x^2)^{1/2}(1+2x^2) - ln\left[x+(1+x^2)^{1/2}\right]\right]\right\}, \tag{3.3.42}$$

$$\mathcal{P}_\mu = \frac{m_\mu c^2}{\lambda_\mu^3}\left\{\frac{1}{8\pi^2}\left[x(1+x^2)^{1/2}(2x^2/3 - 1) + ln\left[x+(1+x^2)^{1/2}\right]\right]\right\}, \tag{3.3.43}$$

where

$$\lambda_\mu = \frac{\hbar c}{m_\mu c^2}\,, \tag{3.3.44}$$

and,

$$x = \frac{(3\pi^2 n_\mu)^{1/3}\hbar c}{m_\mu c^2}. \tag{3.3.45}$$

In chapter 4 the condition of beta-equilibrium will be investigated in detail in order to compute exactly the values of n_i and δ to be inserted in previous equations.

Chapter 4

Theoretical predictions and observational constraints

The aim of the present work is to investigate the main properties of a neutron star, in particular we are interested in its mass-radius relation. In addition, thanks to gravitational wave observations as of 2017, additional data regarding the structure of neutron stars are available, for the purposes of our work we focused in particular on the parameters k_2 (tidal love number) and Λ (tidal deformability) for which through our models we are able to make predictions.

4.1 Solving TOV equations using numerical methods

The best tool consistent with general relativity that we have for making predictions on masses and radii of neutron stars are the TOV equations described in Chapter 3, they cannot be analitically integrated so it's necessary to develop a numerical code capable to perform such computations. Using ODEINT routine in Python we solved 3.1.9 and 3.1.10, two coupled second order differential equations for pressure and mass, both depending on the radial coordinate. The results of mass and radius for a neutron star are also defined by the boundary conditions, in particular the mass must be zero for $r = 0$ and also some value must be chosen for the central pressure $P(r = 0)$. Different values of mass and radius are obtained by varying the pressure $P(r = 0)$ at the center of the star. Because of the structure we gave to our code, we didn't change $P(0)$ directly but we changed the value of baryonic density on which pressure depends in a range between $n = 0.05\text{fm}^{-3}$ and a n_{max}. The latter is different for each parametrization, there is indeed a certain threshold for n beyond which the results do not converge. The density n_{max} is generally between 1.4fm^{-3} and 1.8fm^{-3}. Hence for any choice of central pressure, by stopping numerical integration when the pressure changes sign, one gets the corrisponding radius R which coincides with the edge of the star. This computation also yields a mass value $\mathcal{M}(R)$, which in fact represents the mass of the neutron star.
The need for TOV equations in place of the classical one for hydrostatic equilibrium it's clear since the general relativity term (GR) $(1 - 2Gm/(rc^2))$ is not negligible for high compactness parameters (see Chapter 3) as the ones encountered in neutron stars. Recalling also that to be integrated, TOV equations require an equation of state

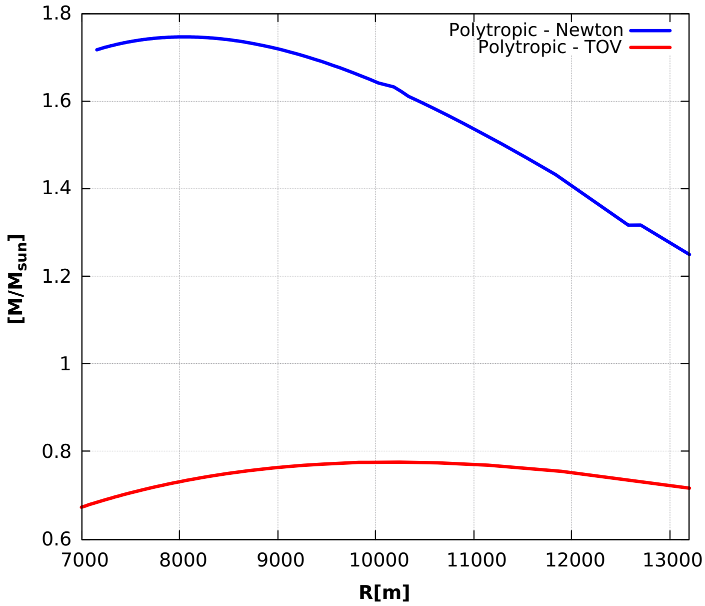

Figure 4.1: Predictions of mass-radius relation in a simple polytropic model, using Netwtonian gravity (blue) and General Relativity (red).

that returns an energy density value associated with each pressure value, this suggests that a crucial part of the code will consist precisely in generating such a function, either in analytical or numerical form. In Fig. 4.1 we have reproduced results in [47] considering the trivial model of polytropic EoS for a relativistic Fermi gas following the idea in the original work of Oppenheimer and Volkoff [48]. Implementing first classical equations then TOV ones observes how much the general relativity corrections are determining in our results. In addition it is also clear from TOV results that nuclear interactions will be instrumental for describing observations.

Our approach has been that of building the EoS numerically, the idea is the following: First consider equation 3.3.1 for the total energy density togheter with the analog one for pressure:

$$\mathcal{P} = \mathcal{P}_{nucl} + \mathcal{P}_{\mu} + \mathcal{P}_{elec}. \tag{4.1.1}$$

We emphasize that mass terms in 3.3.1 give zero contribution to pressure.

Not considering muons at first, our procedure involves generating a table of values of $\mathcal{E}$ and $\mathcal{P}$ which depend on n (baryonic density) and δ (asymmetry coefficient), the latter has to be computed at each step in order to satisfy beta-equilibrium condition at any density (next section will be dedicated to this topic), for a range of density values n running from $10^{-5}\mathrm{fm}^{-3}$ to $1.8\mathrm{fm}^{-3}$ with a step of $10^{-5}\mathrm{fm}^{-3}$. It is not necessary to generate values at lower baryonic densities; the reason will be discussed later. Since pressure increases monotonically with n, and so is the total energy density, one can make a table in which for a fixed n, a value of pressure is associated to a value of the energy density, such a biunivocal relation constitutes the equation of state. Finally, by means of an interpolating function, one gets a function which returns an energy density for any given pressure.

At last notice that central densities in TOV integration are not chosen equally spaced in the interval $0.05\text{fm}^{-3} < n < n_{max}$ since the points in the mass-radius graph get narrower for values corresponding to low baryonic densities, then to produce a graph with a satisfying number of points even at high masses, one have to choose a major number of high n_{cen} (central baryonic density) than lower ones.

4.2 β-equilibrated npe matter

We have already pointed out the dependence of 3.3.23 on two parameters n and δ, in this section we focused on the latter, in particular on what requirements do constraint it, i.e., beta equilibrium and charge neutrality.
The process allowing to convert protons and neutrons into each other is beta decay which can be described with the relation:

$$p + e^- \rightleftharpoons n + \nu_{e^-} \, . \tag{4.2.1}$$

In the $T \to 0$ limit, one can work in the "Fermi-surface (FS) approximation" where the Urca processes (reactions in which a neutron star cools by neutrino emission) are dominated by nucleons and electrons close to their Fermi surfaces [49]. For such a system to be in equilibrium with respect to weak interactions the requirement is

$$\mu_n - \mu_p = \mu_e \, , \tag{4.2.2}$$

having considered zero the energy density contribution of neutrinos since at temperatures low enough the neutrino mean-free path is larger than the size of the star [50]. The chemical potentials of different species $\mu_i = \partial\mathcal{E}/\partial n_i$ corresponds to the energy gain or loss in adding or subtracting one particle of that species to the system. The computation for μ_e can be performed easily starting from 3.3.40 to obtain

$$\mu_e = \hbar c \left(3\pi^2 n_e\right)^{1/3} \, , \tag{4.2.3}$$

while for the terms regarding neutrons and protons, it can be derived a simple relation departing from $2n_p = (1-\delta)n$ and $2n_n = (1+\delta)n$ following the definition of delta 3.3.22. Since the expressions for energy densities are all given as functions of n and δ instead of n_n and n_p, is preferable to convert the derivative $\partial\mathcal{E}/\partial n_n - \partial\mathcal{E}/\partial n_p$ into one with derivatives in the other two variables, hence it can be observed:

$$\begin{aligned} \frac{\partial}{\partial n_n} &= \frac{\partial \delta}{\partial n_n}\frac{\partial}{\partial \delta} + \frac{\partial n}{\partial n_n}\frac{\partial}{\partial n} \\ \frac{\partial}{\partial n_p} &= \frac{\partial \delta}{\partial n_p}\frac{\partial}{\partial \delta} + \frac{\partial n}{\partial n_p}\frac{\partial}{\partial n}, \end{aligned} \tag{4.2.4}$$

subtracting the two lines in 4.2.4 from each other, we obtain

$$\frac{\partial}{\partial n_n} - \frac{\partial}{\partial n_p} = \frac{\partial}{\partial \delta}\left(\frac{\partial \delta}{\partial n_n} - \frac{\partial \delta}{\partial n_p}\right) \, , \tag{4.2.5}$$

where two terms cancel out since $n = n_n + n_p$; using finally the expression for δ (Eq.3.3.22) to compute $\partial\delta/\partial n_i$ we get to the easier formula:

$$\frac{\partial}{\partial n_n} - \frac{\partial}{\partial n_p} = \frac{2}{n}\frac{\partial}{\partial \delta} \, . \tag{4.2.6}$$

The two derivatives with respect to n_n and n_p are now reduced to only one derivative in δ at fixed n. This result can be deployed to obtain an equation for delta, indeed equating the expression for μ_e and the one for $\mu_n - \mu_p$ as in 4.2.2 one obtains

$$\hbar c \left(3\pi^2 n_e\right)^{1/3} = \frac{2}{n}\frac{\partial\,(E/A)\,n}{\partial\delta}\,. \tag{4.2.7}$$

Considering now Skyrme type interactions, by entering the expression for E/A 3.3.23 in non-approximated form into 4.2.7 and doing some calculations one gets:

$$\begin{aligned}\hbar c \left(3\pi^2 n_e\right)^{1/3} = &\frac{\hbar^2}{2m}\left(\frac{3\pi^2}{2}\right)^{2/3} n^{2/3}\{(1+\delta)^{2/3} - (1-\delta)^{2/3}\}\\ &- \frac{1}{2}t_0 n\delta(2x_0+1) - \frac{1}{12}t_3 n^{\sigma+1}\delta(2x_3+1)\\ &+ \frac{1}{8}\left(\frac{3\pi^2}{2}\right)^{2/3}\left[t_1(2+x_1)+t_2(2+x_2)\right] n^{5/3}\{(1+\delta)^{2/3}-(1-\delta)^{2/3}\}\\ &+ \frac{1}{10}\left(\frac{3\pi^2}{2}\right)^{2/3}\left[t_2(2x_2+1)-t_1(2x_1+1)\right] n^{5/3}\{(1+\delta)^{5/3}-(1-\delta)^{5/3}\}\,.\end{aligned} \tag{4.2.8}$$

This is an equation in the only variable δ once n is fixed that cannot be solved analytically, anyway it can be easily solved numerically by our code (alternatively one can consider the approximate expression of $E/A(n, \delta)$ truncated to second order in δ (Eq.3.3.26) and thus obtain an analytically solvable third-degree equation).
The implementation of this constraint in the code which returns a value for δ together with the charge neutrality $n_p = n_e$, allows to compute the correct values of energy density and pressure at any density n.
Fig.4.2 shows, considering SLy4 parametrization, how δ varies as a function of the baryonic density, from which one can immediately compute n_e, n_p, n_n satisfying beta-equilibrium, and consequently even the energy per nucleon E/A as showed in Fig.4.3 in different cases, namely those of SNM (symmetric nuclear matter), PNM (pure neutron matter), BEM (beta equilibrated matter). See [35; 9; 51] for a comparison of the results obtained using SLy4 and other parametrizations.

4.3 Effects due to second order approximation of energy on mass and radius

One might wonder how valid is the quadratic approximation described in the equation 3.3.26. The expansion around $\delta = 0$ of the expression of the energy per nucleon, contains only terms of even powers. It can be seen, in fact, that the complete expression of $E/A(n, \delta)$ 3.3.23 is completely symmetric with respect to δ, so the second nonzero term in the expansion is that of order 4. As mentioned in Chapter 3 several references note how this term is negligible for any value of baryon density in the range investigated in the context of neutron stars.
The quadratic approximation makes it possible to greatly lighten the calculations of

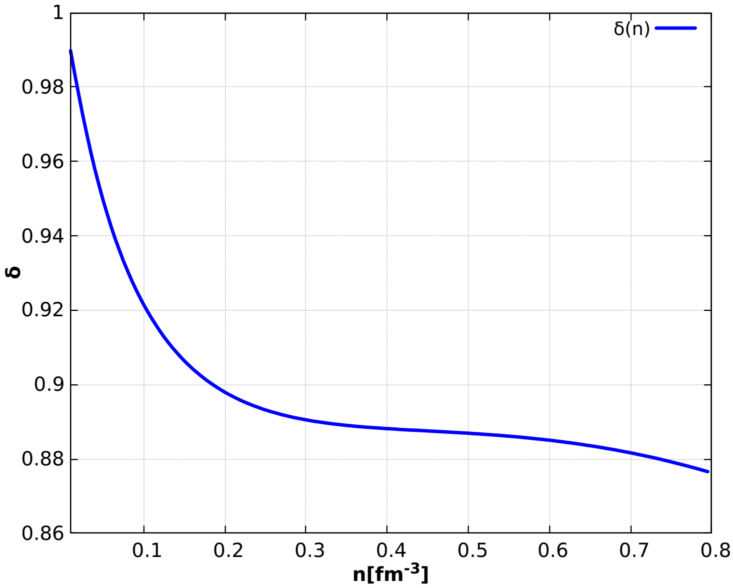

Figure 4.2: Values of δ found by imposing beta equilibrium condition at different values of n using SLy4 Skyrme parametrization.

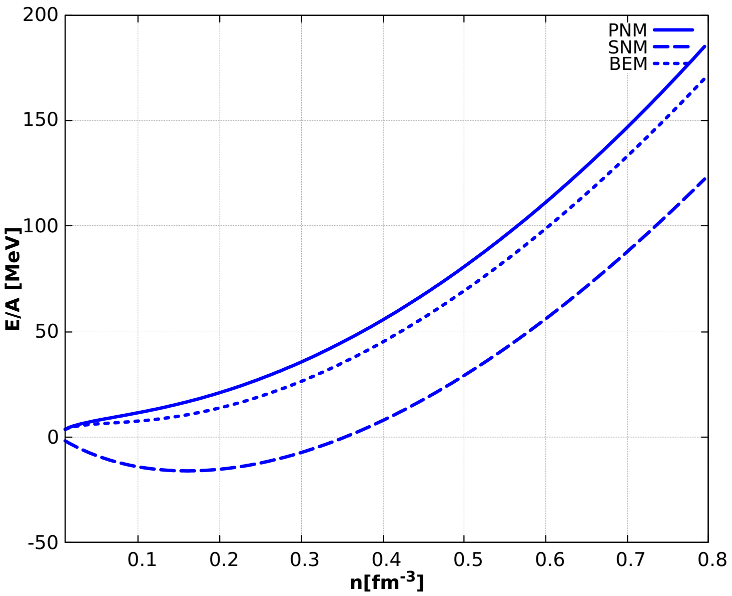

Figure 4.3: Energy per baryon using SLy4 Skyrme parametrization in different scenarios: PNM (pure neutron matter), SNM (symmetric nuclear matter), BEM (beta equilibrated matter).

the various energy and pressure expressions used to construct the equation of state. In particular, it is effective in simplifying the expression by which δ is derived under the assumption of beta-equilibrium matter for which an analytical expression can be derived instead of a numerical one. Below we report the differences in the calculations from those described in the previous section for the non-approximate treatment.
Using the equation 3.3.26 where E_{sym} is described in 3.3.27 one can perform calculations similar to those described in the section on beta-equilibrated npe matter. The equation for beta-equilibrium is once again

$$\mu_e = \mu_n - \mu_p\,, \tag{4.3.1}$$

where μ_e is the same of Eq. 4.2.3, but the right hand side takes a different form, indeed using 4.2.6 on the approximated $E/A(n,\delta)$ one gets a simple relation:

$$\mu_n - \mu_p = 4E_{sym}(n)\delta\,, \tag{4.3.2}$$

which can be inserted in the equation for beta-equilibrium together with the expression for μ_e to get

$$\hbar c \left(3\pi^2 n_e\right)^{1/3} = 4E_{sym}(n)\delta. \tag{4.3.3}$$

The last equation can be rewritten as:

$$\delta^3 + \delta\left[\frac{3\pi^2}{2}\left(\frac{\hbar c}{4E_{sym}}\right)^3 n\right] - \left[\frac{3\pi^2}{2}\left(\frac{\hbar c}{4E_{sym}}\right)^3 n\right] = 0\,, \tag{4.3.4}$$

which has the form of a third degree equation in δ:

$$\delta^3 + X(n)\delta - X(n) = 0\,. \tag{4.3.5}$$

After having defined,

$$X(n) \equiv \frac{3\pi^2}{2}\left(\frac{\hbar c}{4E_{sym}}\right)^3 n\,. \tag{4.3.6}$$

Finally, using the solving formula for third degree equations one gets the prescription for calculating δ:

$$\delta = \sqrt[3]{\frac{X(n)}{2} + \sqrt{\frac{X(n)^2}{4} + \frac{X(n)^3}{27}}} + \sqrt[3]{\frac{X(n)}{2} - \sqrt{\frac{X(n)^2}{4} + \frac{X(n)^3}{27}}}\,. \tag{4.3.7}$$

It is therefore easy to see that for each value of n it is possible to calculate δ for beta-equilibrium and consequently the expressions for the energy density and pressure related to the nucleonic part. In this way an equation of state is constructed as described in the first paragraph of this chapter to be included in the TOV equations. Fig. 4.4 demonstrates what was stated above about the goodness of the quadratic approximation of energy per nucleon in predicting mass and radius of neutron stars, the differences are practically negligible. However, in the remainder of the thesis the full expression for a non-approximation of the studied observables will be implemented.

4.4 BPS EoS and the merging problem

The nuclear matter model we used in the present work falls into the category of non-unified EoS, that is, those built by "patches", where each part is derived from

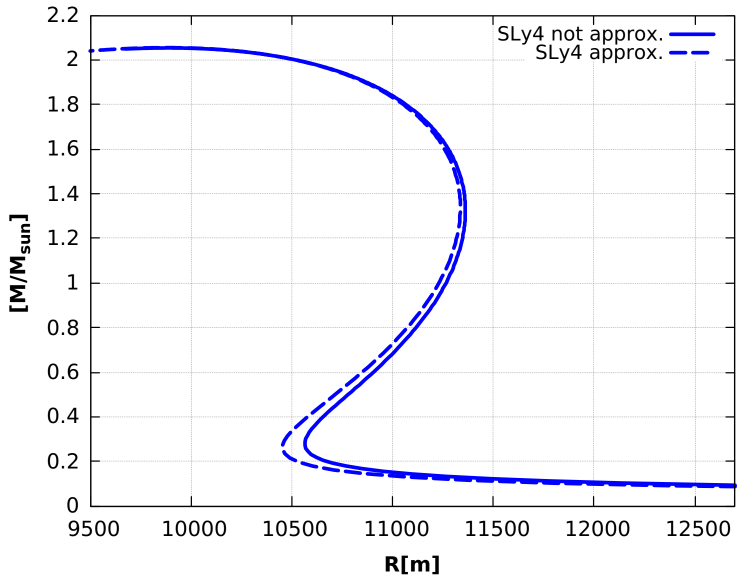

Figure 4.4: Mass and radius computed using the approximated expression 3.3.26 for the energy per baryon, and the non-approximated one 3.3.23 with SLy4 parametrization.

a model that is essentially different from the one used to build the other. Matter within neutron stars, indeed, varies over a wide range of densities, starting from zero up to densities several times higher than the saturation density $n_0 = 0.16\text{fm}^{-3}$. As described in Chapter 2 a neutron star consists of several layers, particularly focusing on the core and crust one can wonder how the EoS changes between one layer and the other.
In practice for the NS crust, where $\rho < 10^{11}\text{g cm}^{-3}$ experimental data concerning nuclear masses are used, whereas for higher values of the density no measurements are available for the properties of matter when nuclei drip neutrons or start to merge. Therefore it is necessary to use theoretical models such as the one described in Chapter 3 under mean-field theories. In particular, for low densities many authors use the BPS (Baym-Pethick-Sutherland) equation of state [11] combined with the BBP (Baym-Bethe-Pethick) [52]. As mentioned in Chapter 2, in fact, the BPS equation of state is constructed from experimental results of nuclear masses and thus is very accurate for describing matter in the range of typical densities of atomic nuclei.
In [53] it has been shown that using a non-unified EoS hardly affects the determination of the NS mass but has a significant influence on the radius calculation. In particular the choice on how to make the merger between the EoS for the crust (BPS) and the EoS for the core (Skyrme) involves uncertainties that can be as large as 30% for the crust thickness and 4% for the radius.
In our code we have implemented a function that performs merging between the two EoS, exactly at the point of intersection between the two curves. In Fig. 4.5 it can be seen that at each value of baryon density, the EoS between the two that has less energy is used, which therefore a priori stabilizes the system at most. More in detail by defining P_{match} the pressure value at which the two curves intersect, we consider

P_1 the last value tabulated in the original BPS article, while for the Skyrme part it is possible to calculate the energy density value for any pressure, consequently with a cubic order interpolation we obtain the part of the equation of state between P_1 and P_{match}.

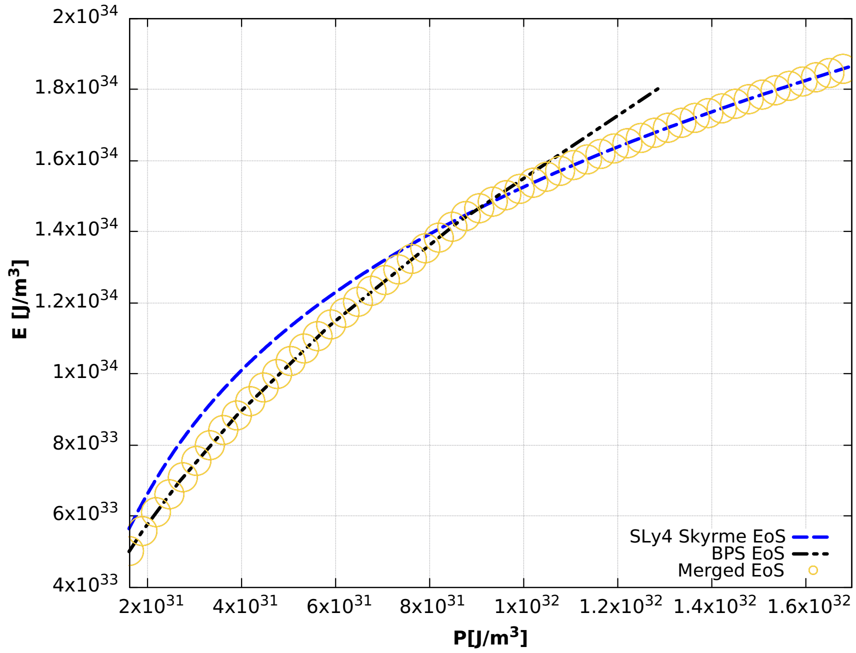

Figure 4.5: Merging between BPS and SLy4 Eos.

It is shown in Fig. 4.6 how the results for the mass-radius graph vary depending on the choice on how to perform the merging, as analyzed in detail in the aforementioned article [53]. It is shown that indeed the mass values are practically unaffected by this choice; on the contrary, the curve shifts continuously toward smaller radii as the merging point, i.e., the pressure value from which the Skyrme EoS is considered instead of the BPS, is shifted to lower pressures. There is no predefined criterion for doing merging; other ways besides the one we choose can be used.
In any case, the constraint of subluminality must always be respected and checked by our code; in fact, one can define the speed of sound in nuclear matter at constant entropy s by the expression:

$$c_s^2 \equiv \left(\frac{\partial P}{\partial \mathcal{E}} \right)_s , \tag{4.4.1}$$

which obviously cannot exceed the speed of light (causality). This property is already satisfied by construction for BPS and Skyrme EoS we used, but it is not a priori verified in the interpolation part between the two. One could indeed interpolate two curves arbitrarily, among the various possible ways, some could show curves with a slope $(\partial P/\partial \mathcal{E})$ greater than 1.
We have also noticed that our results are not very sensitive to changes in the "exit value" at least up to a pressure of $\sim 10^{23} \mathrm{J/m}^3$, this happens because near the value of r at which the integration stops, i.e. getting to zero pressure point,the pressure

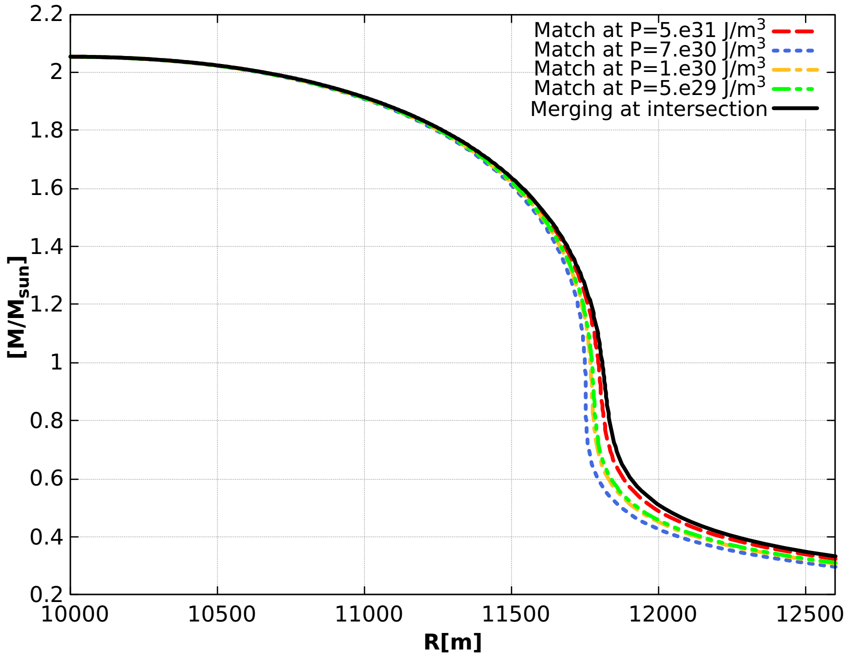

Figure 4.6: Changes in radius choosing different matching points between BPS EoS and SLy4.

changes very rapidly, from values around $10^{24}\mathrm{J/m^3}$ to negative ones in 2-3 integration steps. Having chosen $dx = 3\mathrm{m}$ as the integration step, there's no big difference in choosing values not too many orders of magnitude greater than $10^{21}\mathrm{J/m^3}$ as the exit value (see Fig. 4.7) for pressure, this make the computation of the EoS lighter since there's no need to compute it for values of n lower than $10^{-5} - 10^{-6}\mathrm{fm^{-3}}$. One explanation for this fact may be attributed to the fact that the central pressures for neutron stars vary in a range between $10^{31}\mathrm{J/m^3}$ and $10^{35}\mathrm{J/m^3}$, while the output pressures are significantly lower, and thus the difference between an output value 10 orders of magnitude less than the central pressures and one less than 7 orders of magnitude is not appreciable by the numerical code.

4.5 Muons contribution: β-equilibrated $npe\mu$ matter

Let us now consider the need to introduce muons into our model. At high densities new particles can be produced from npe matter, so that the lowest-energy configuration is reached.
Normally muons decay into electrons by,

$$\mu^- \longrightarrow e^- + \nu_\mu + \bar{\nu}_e \,. \tag{4.5.1}$$

However, when the Fermi energy of the electrons, which increases with increasing density, approaches the muon mass energy at rest $m_\mu \simeq 105.66$ MeV, it is energetically

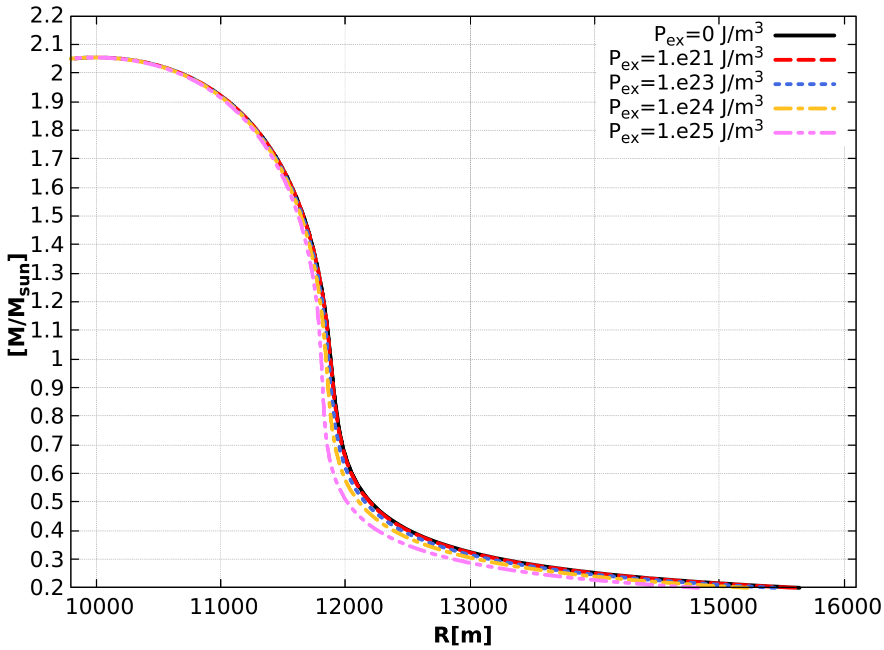

Figure 4.7: Predictions of mass-radius relation using SLy4 Skyrme, with different exit conditions on pressure.

more convenient for electrons closer to the Fermi surface to decay into muons, with the emission of neutrinos and antineutrinos. The latter escape from the star so we will consider all quantities concerning neutrinos to be zero in our calculations. From a certain density upward, therefore, electrons and muons will be present in matter in equilibrium with each other. This condition is expressed by the equality of chemical potentials,

$$\mu_e = \mu_\mu \,. \tag{4.5.2}$$

As just mentioned, the condition indicating the baryon density $\widetilde{n}$ value at which muons are to be considered is given by:

$$\mathcal{E}_{elec}(n) > \mathcal{E}_\mu(n) \,, \tag{4.5.3}$$

where the two expressions of energy density are given by equations 3.3.40 and 3.3.42. When constructing the equation of state, it is therefore necessary for the code to check for each value of baryon density whether the condition 4.5.3 is verified or not.
In order to have beta-equilibrium together with charge neutrality, reminding that muons have negative charge, the following equations must be verified simultaneously:

$$\begin{cases} \mu_n - \mu_p = \mu_e \\ \mu_e = \mu_\mu \\ n_n + n_p = n \\ n_p = n_e + n_\mu \,. \end{cases} \tag{4.5.4}$$

Since the chemical potentials for each type of particle depend on the density of particles of that type, one can write the inverse relationship and find each of the $n_i = n_e, n_p, n_n, n_\mu$ as a function of the chemical potentials and the parameter δ. Reminding that:

$$\mu_e = \hbar c(3\pi^2 n_e)^{1/3} = (\mu_n - \mu_p)\,, \tag{4.5.5}$$

and,

$$\mu_\mu = m_\mu c^2 \sqrt{1 + \left[\frac{\hbar\left(3\pi^2 n_\mu\right)^{1/3}}{m_\mu c}\right]^2} = (\mu_n - \mu_p) \tag{4.5.6}$$

the following system is obtained in the variables n and δ only:

$$\begin{cases} n_e = \dfrac{(\mu_n - \mu_p)^3}{\hbar^3 c^3 3\pi^2} \\[2ex] n_\mu = \left[\dfrac{(\mu_n - \mu_p)^2}{m_\mu^2 c^4} - 1\right]^{3/2} \times \left(\dfrac{m_\mu^3 c^3}{3\pi^2 \hbar^3}\right) \\[2ex] n_p = \dfrac{n}{2}(1-\delta) \\[2ex] n_n = \dfrac{n}{2}(1+\delta)\ . \end{cases} \tag{4.5.7}$$

The results of the system 4.5.7 can be plotted in a graph expressed as a fraction of the total baryon density, $y_i = n_i/n$ as in Fig. 4.8.
Finally, by entering the last result obtained in the fourth line of the system 4.5.4 one gets:

$$\frac{n}{2}(1-\delta) = \frac{(\mu_n - \mu_p)^3}{\hbar^3 c^3 3\pi^2} + \left[\frac{(\mu_n - \mu_p)^2}{m_\mu^2 c^4} - 1\right]^{3/2} \times \left(\frac{m_\mu^3 c^3}{3\pi^2 \hbar^3}\right)\,, \tag{4.5.8}$$

which can be solved numerically to find the values of δ for any fixed n.
Having at this point all the density values for each type of particle and the δ asymmetry parameter at a fixed n, it is possible to compute the total energy density and pressure values (see Fig. 4.9) (containing the contributions from nucleons, electrons and muons) and thus obtain a new equation of state.
Obviously, each Skyrme shows different behavior when muons are taken into account; for example, SLy4 shows little sensitivity to this type of correction, while other parameterizations such as SkI3 show more significant differences than the case without muons as can be seen from Fig. 4.10.
From Fig. 4.10 it can also be seen from the mass-radius graph that the correction resulting from the addition of muons always leads to a decrease in both the mass and radius quantities. This is due to the fact that muons "take away" kinetic energy from the system in the form of mass energy. In other words, the system favors the production of "mild relativistic" muons (for which most of the energy is mass energy rather than kinetic energy and thus contribute very little to the pressure) instead of further increasing the kinetic energy of the electrons present, which instead contribute more to increasing the pressure. As a final result the overall pressure will be reduced

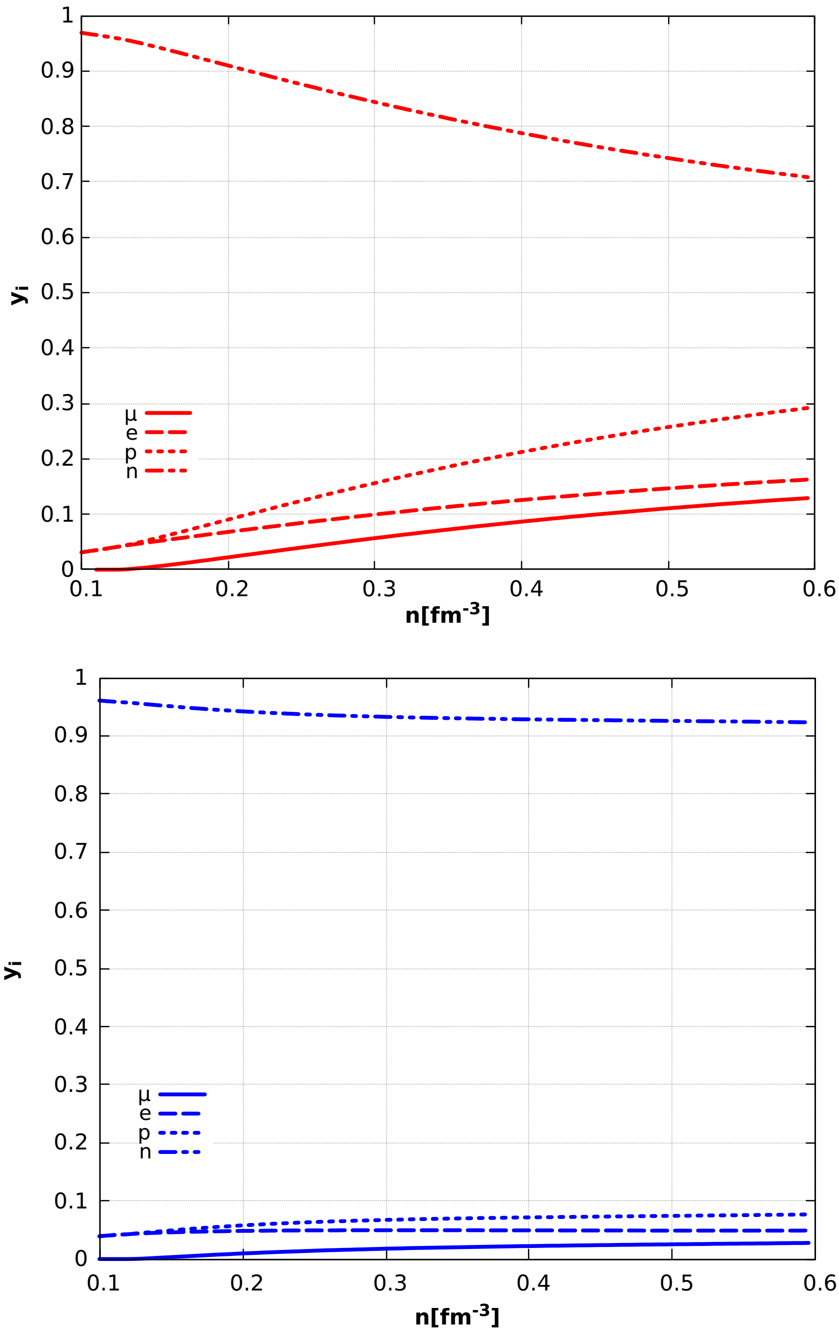

Figure 4.8: Particles fractions in beta-equilibrated $npe\mu$ matter at different baryonic densities for SkI3 EoS (above) and for SLy4 EoS (below).

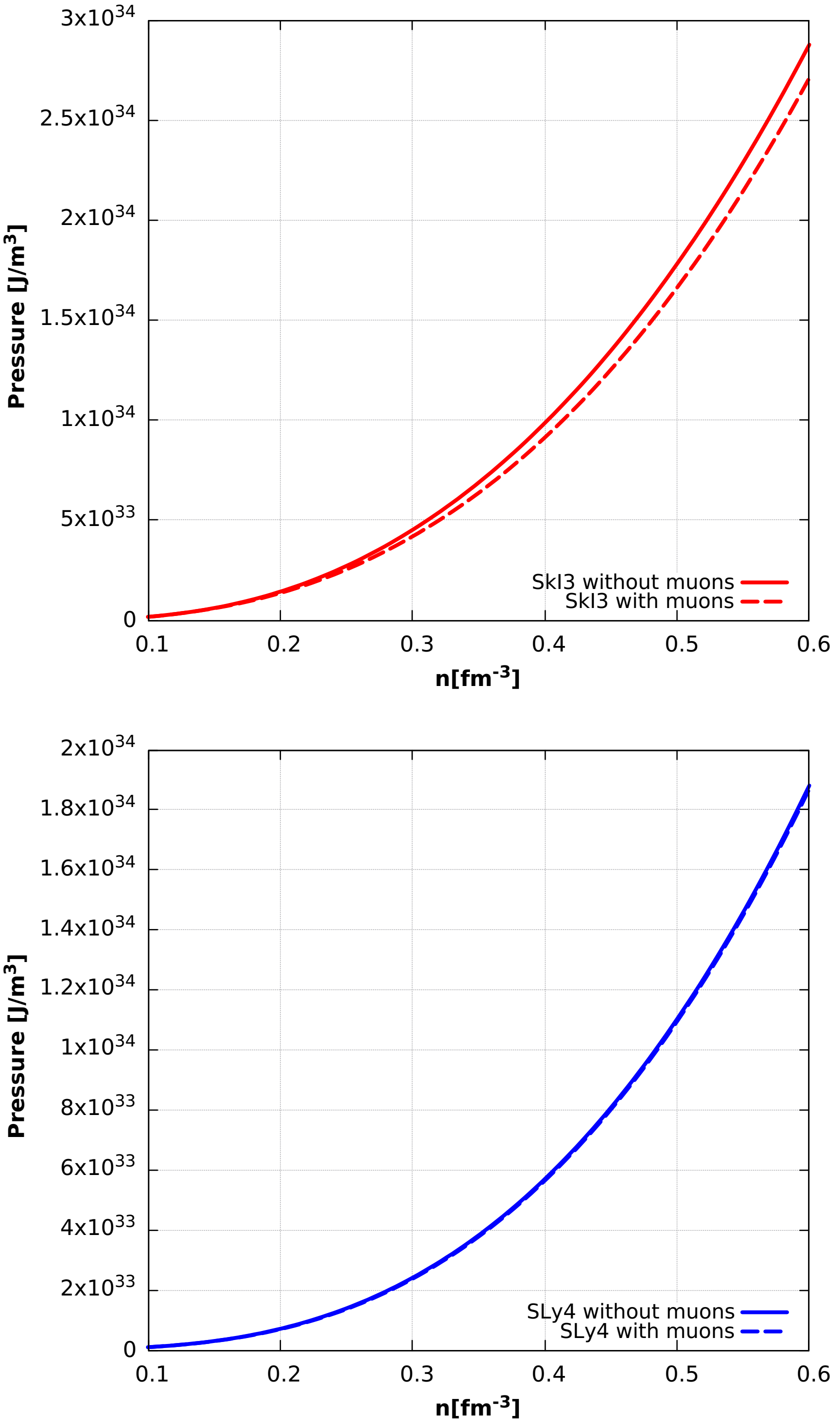

Figure 4.9: Pressure at different baryonic densities for SkI3 EoS (above) and for SLy4 EoS (below) in beta-equilibrated $npe\mu$ matter.

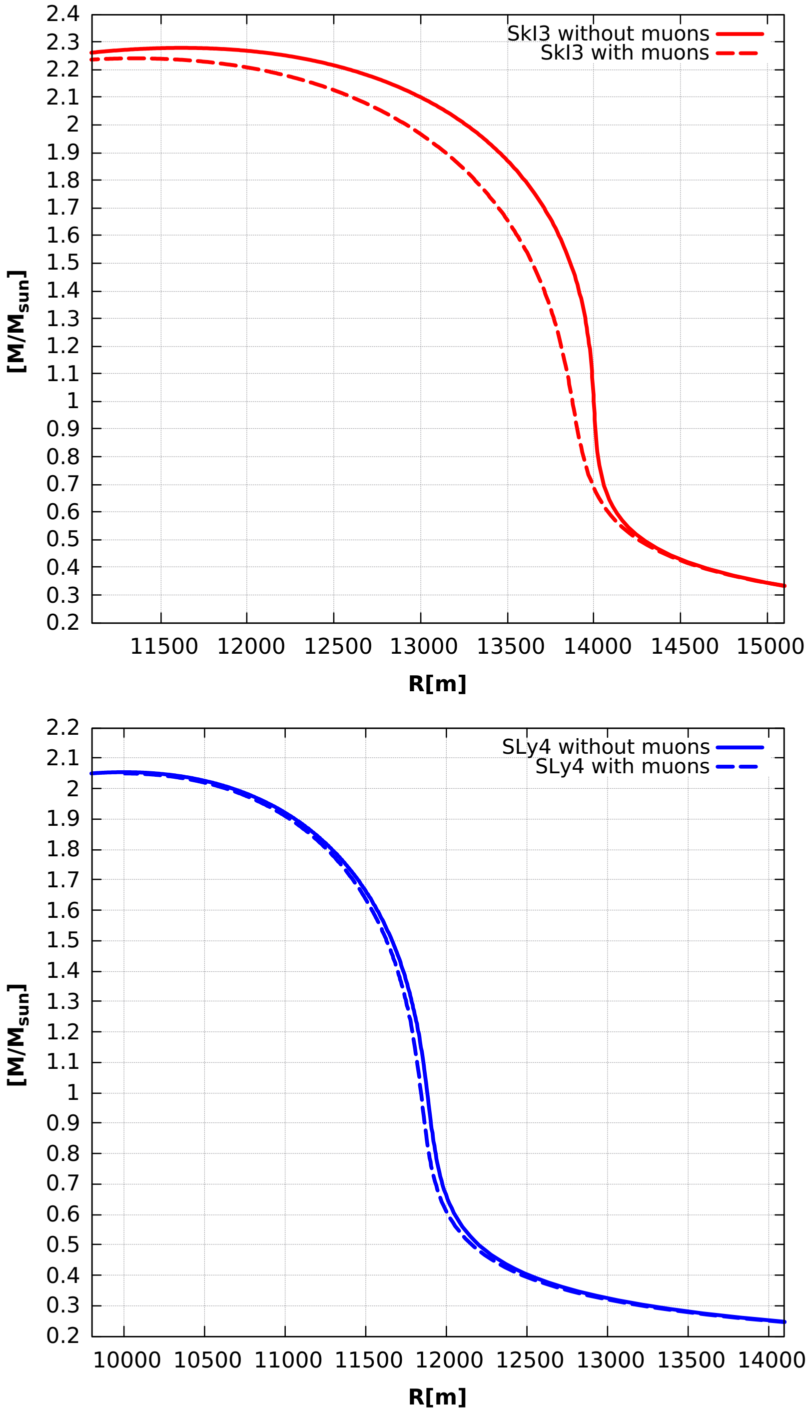

Figure 4.10: Mass-radius plot using SkI3 (top) and SLy4 (bottom) merged with BPS EoS considering muon contribution.

compared to the case without muons.

4.6 M-R results for SAMi-J Skyrme and Fayans functional

Having a code that can implement all the features described in the previous paragraphs, it is possible to compare the results with those available in the literature for the most studied parameterizations (e.g. SLy4, SkI3, SkO...) [35].
Therefore, in the present work, we have focused on theoretical predictions regarding neutron stars, which can be obtained using parameterizations resulting from a collaboration between the University of Milan and Aizu University, known as SAMi [54]. The SAMi parameterization is calculated using a protocol similar to that used for SLy, but with an improved description of the spin-isospin properties. SAMi-J has been demonstrated to be effective in predicting the GTR (Gamow-Teller resonance) phenomenon in certain nuclei.
In particular, we used the Skyrmes belonging to the SAMi-J family, obtained using the same protocol from the original SAMi and varying only the symmetry energy J at saturation density n_0 (for SAMi-J29 J = 29MeV, and so on) keeping fixed the values of the nuclear incompressibility ($K_\infty = 245$ MeV) and the effective mass ($m^*/m = 0.675$) [55]. This allows to study the predictions of a model that keep fixed isoscalar properties while systematically varying isovector properties.
The results for mass-radius relation obtained using these parameterizations can be observed in Fig. 4.11.
There is actually an empirical relationship between the two parameters

$$J \equiv E_{sym}(n_0)\,, \tag{4.6.1}$$

and,

$$L \equiv 3n(\partial E_{sym}/\partial n)\big|_{n=n_0}\,, \tag{4.6.2}$$

that is the slope of the symmetry energy evaluated at saturation density.
In the reference [56] it is shown how in a model-independent manner the graphs of symmetry energy as a function of density n intersect at a density $n^* = 0.105$ fm^{-3} corresponding to an $E^*_{sym} = 25.7$ MeV. By expanding in Taylor series the function for the symmetry energy around n_0 and considering only the linear term, one finds a relation between J and L of the type,

$$L = 10(J - E^*_{sym})\,. \tag{4.6.3}$$

It is thus shown that in the neighborhood of n^* the parameter L increases with J.
It can also be seen in the figure that as J increases, the mass-radius curves show increasing values for both mass and radius. This can be justified by what has just been explained, namely, that at saturation density parameter L grows along with parameter J, but in turn L is related to pressure by the relation $P_{nucl}(n_0) = n_0(L/3)$ [57]. It follows immediately then that for the same density (n^*), higher values of J correspond to higher pressures. In relatively simple models, though, we can assume that an EoS that is stiff at saturation density continues to be stiff even at higher densities. Consequently as J gets higher, one expects stiffer EoS and thus higher

mass-radius values.
In Fig. 4.11 the constraints from astrophysical observations described in section 2.2 have been included. As can be seen from the figure, the maximum mass values predicted by the Skyrme SAMi-J vary in a range between 2.10 and 2.20 solar masses, sufficiently in agreement with the constraint given by the most massive neutron star observed so far ($2.35 \pm 0.17 M_{\odot}$), at least for the four SAMi-J models 32, 33, 34, and 35. Our results, for all the SAMi-J models, also satisfy the NICER observations for both the mass and radius ranges. Regarding the constraints from gravitational wave observations, SAMi-J34 and SAMi-J35 do not comply with the maximum radius of 13.76 km predicted for a 1.4 solar mass star as indicated by the analysis of the GW170817 event [5], but all models satisfy the constraint of Bauswein et al [17].
Similarly, the results obtained for the Fayans functional described in Chapter 3 are presented (Fig.4.12); this functional, at least in its original 1998 form, while considered a valid model for the description of nuclear matter, seems in the first instance not to predict results in agreement with experimental observations in the context of neutron stars.
In particular, the maximum mass predicted by the Fayans functional is 1.83 solar masses, and the corresponding radius for a mass of $1.6 M_{\odot}$ is lower than what was observed in [17]. Overall, the equation of state derived from this functional has been found to be too soft, and as a result, a star composed of such matter would not be able to support the masses observed for neutron stars, and would be highly compressed by its own gravity.

4.6.1 Corrections to our results due to rotations

It's noteworthy the fact that observations related to neutron stars' masses used in comparison to predictions of our model have been made on pulsars, which are rapidly rotating neutron stars and this obviously affects the maximum mass a neutron star can sustain thanks to centrifugal force. Therefore by including rotations also our predictions on masses would be corrected toward upper values: see e.g ref [58] where the authors argued that for realistic EOS, maximally rotating neutron stars (that is, rotating at the limiting speed beyond which the star would disintegrate due to centrifugal force.) can support a maximum mass increased by about 20% with respect to the static case. The same paper shows that there exists also a universal relation between the maximum mass of a static and of a maximally rotating configurations. Consider for instance the heaviest and fastest known neutron star: PSR J0952-0607 [6], its spin period is $P_s = 1.41$ms that corresponds to 709 Hz, considering also its mass $M = 2.35 M_{\odot}$, the Keplerian rotation frequency (supposing a radius of 13 km since no available measurements on it) is of the order of 2000Hz. Articles such [59; 60], show calculations on the effects of rotation on masses and radii of neutron stars. It's interesting to note that frequencies around 700 Hz results in corrections of about only $3 - 4\%$ with respect to the static case, and only frequencies near the maximally rotating configurations change significantly the maximum mass values. The last few lines suggest once again the important role of the EoS in our results, even with such extreme rotation velocities the centrifugal contribution is still less relevant than the contribution due to the pressure generated by matter at very high densities. For a more exhaustive treatment of this topic see also [24].

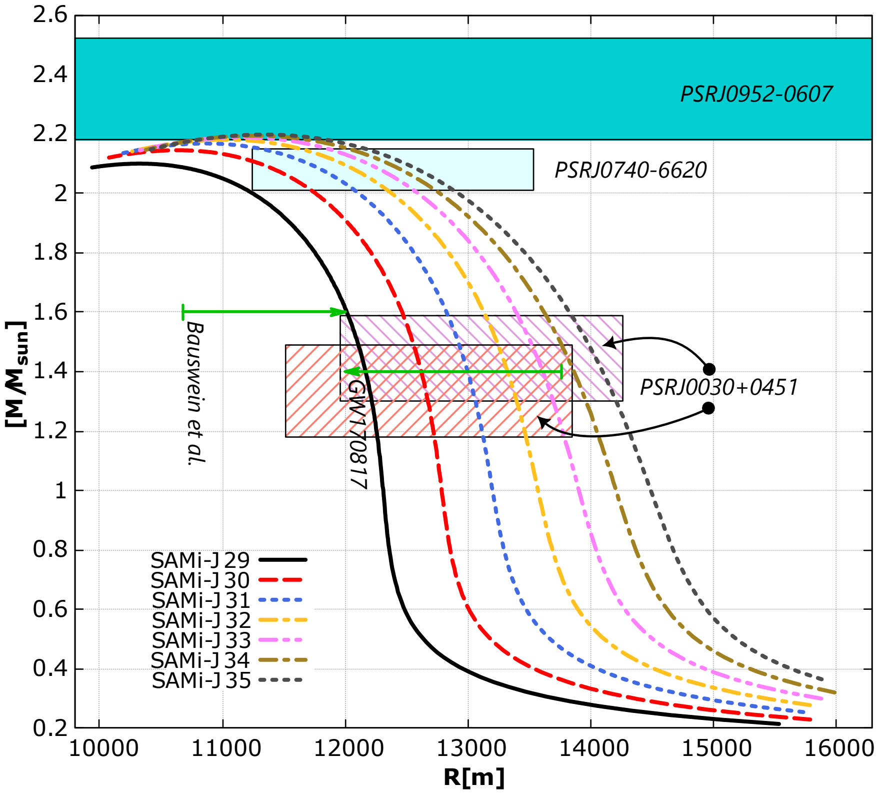

Figure 4.11: Mass-radius relation as predicted by a set of theoretical models belonging to the same family of parametrizations, namely SAMi-J Skyrme. Constraints resulting from astrophysical observations are presented: the three boxes pertain to the two pulsars that were investigated by NICER, for which estimates of both mass and radius are available. For $PSRJ0030 + 0451$, two independent studies have been conducted, and therefore both the results are represented in the figure. The horizontal band concerns the heaviest Pulsar observed so far for which only a mass estimate is available, finally the two arrows are related to constraints from gravitational wave observations.

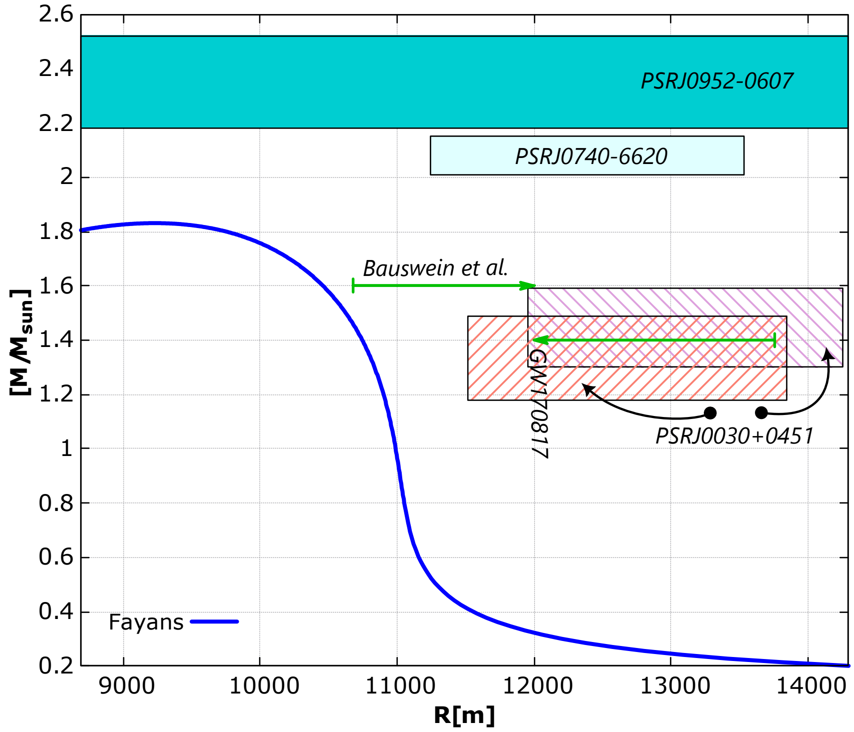

Figure 4.12: Mass-radius relation as predicted by Fayans functional. Constraints due to astrophysical observations are shown as in Fig. 4.11.

4.7 Tidal deformability results for SAMi-J Skyrme and the Fayans functional

This section presents results for Love number k_2 and tidal deformability Λ for the two theoretical models for high-density nuclear matter used in the last section. Recall how the tidal-deformability of a compact object quantifies the quadrupolar deformation of that object under the effect of a tidal field; this observable depends mainly on the compactness parameter $C \propto (M/R)^5$ while it depends to a lesser extent on k_2. In particular, it can be observed from the results previously reported in figures 4.11 and 4.12 how the Skyrme SAMi-J models predict lower compactnesses by at least around 15% (in the case of SAMi-J29) compared to that predicted by the Fayans functional, which translates (by raising to the power of 5) into a difference of at least 85% for the tidal deformability. The graphs related to the parameter k_2 as a function of the ratio M/R are reported in figures 4.13 and 4.14 for completeness, noting that the latter has a moderate dependence on the equation of state, as can be observed by the results obtained for the SAMi-J models which do not differ much from those obtained for Fayans, despite the two models being completely different.

By observing the Λ graph for the SAMi-J models in more detail, it can be seen that as the value of J increases for the various SAMi-J models, the neutron star deformability increases. This can be explained by observing that, as previously noted from the results obtained for $M(R)$, the pressure value at saturation density (and consequently at any density) increases as J increases. As a result, the star is better able to resist compression due to gravity and is therefore less compact, that is, more deformable.

In addition, the observational constraint derived from the GW170817 event has been included in the figures 4.14 and 4.13. For this particular observed system, it has been established that the tidal deformability Λ must be less than 800 for a neutron star with a mass of 1.4 solar masses. This constraint is perfectly respected by all the models used except for the Skyrme SAMi-J35.

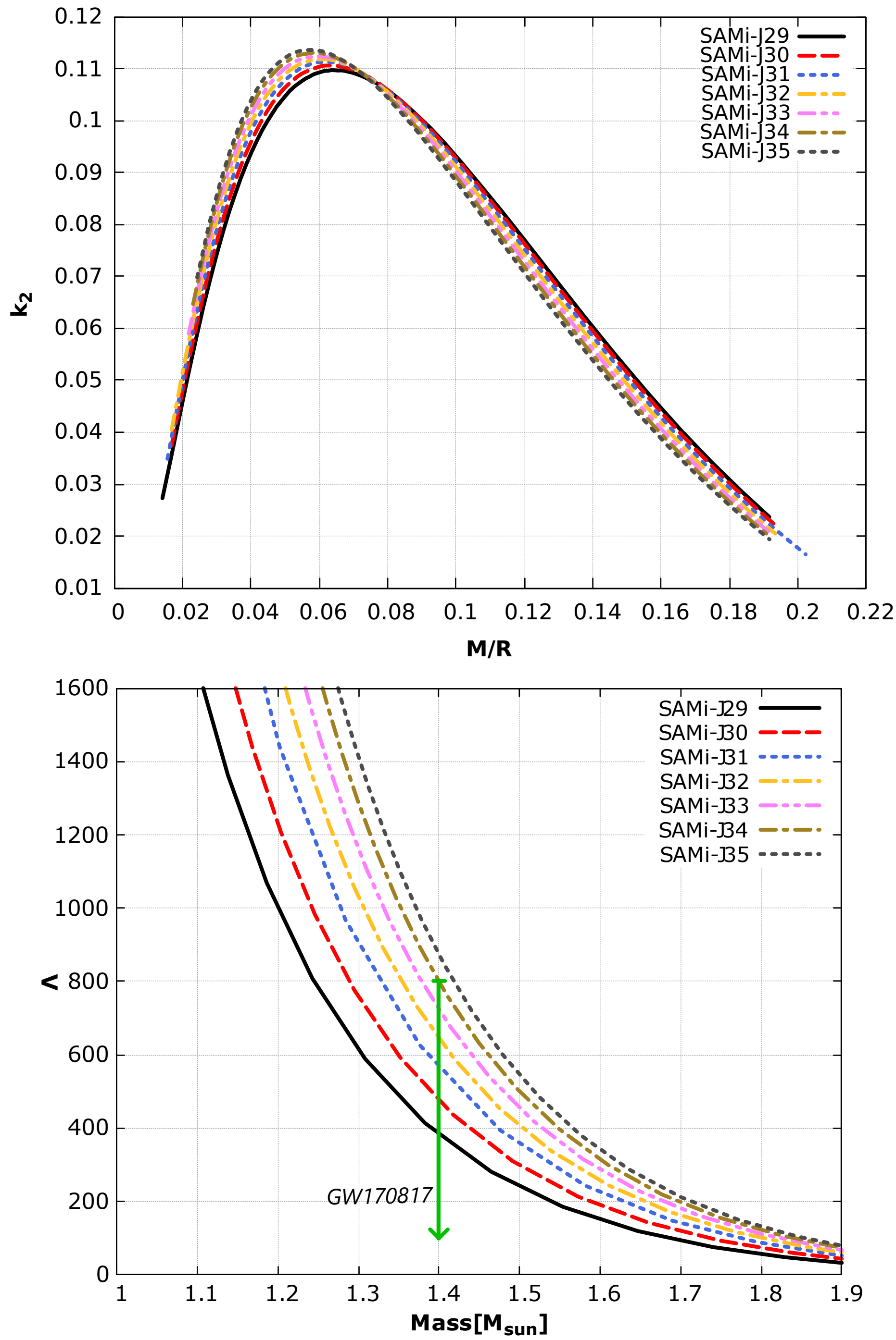

Figure 4.13: k_2 Love number as a function of M/R ratio (mass in units of $M_\odot$, and radius in km) (top) and tidal deformability Λ as a function of mass (bottom) as predicted by SAMi-J Skyrme models. Constraint due to gravitational waves observations is also shown (green arrow).

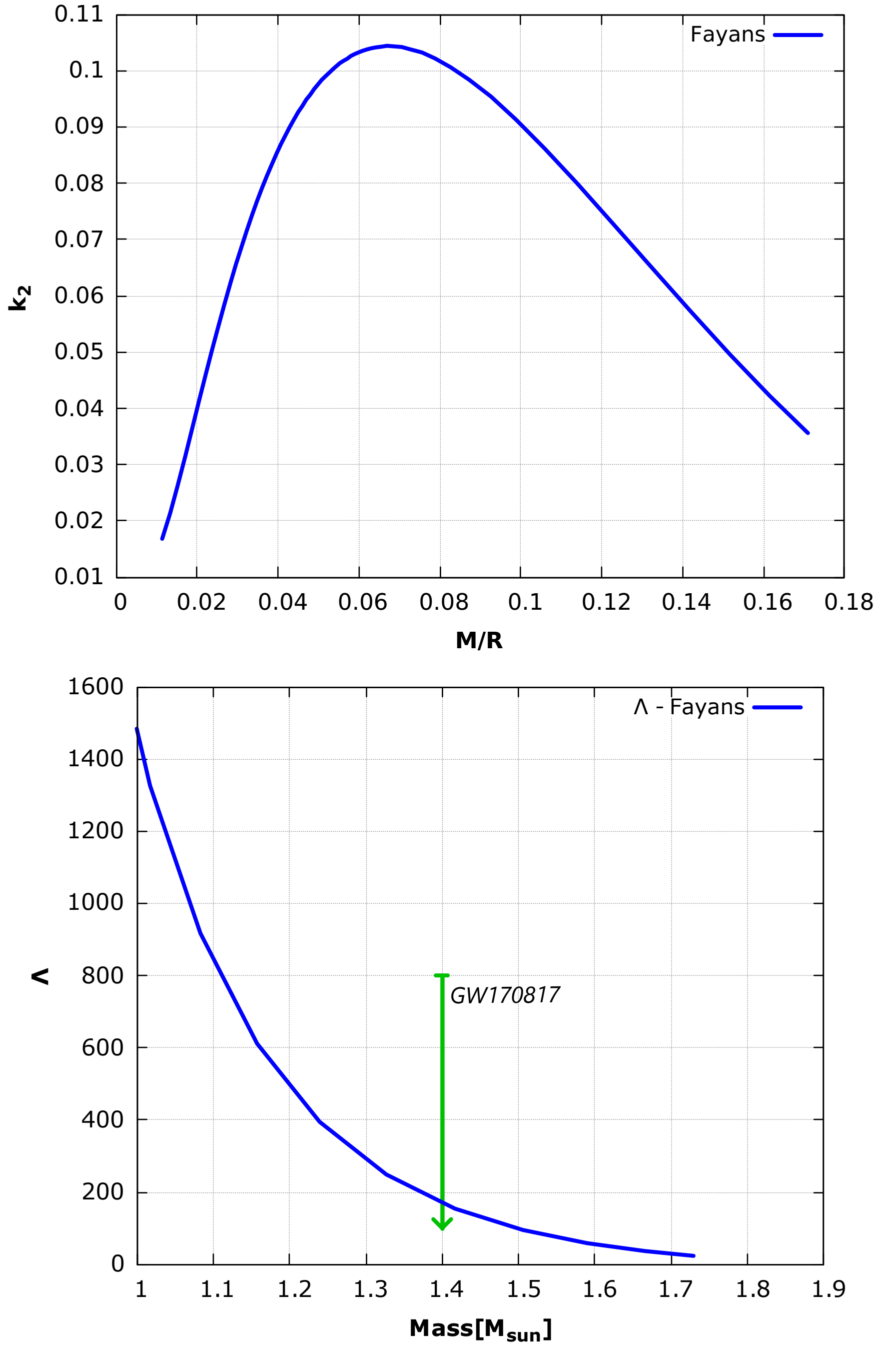

Figure 4.14: k_2 Love number as a function of M/R ratio (mass in units of $M_\odot$, and radius in km) (top) and tidal deformability Λ as a function of mass (bottom) as predicted by Fayans functional model. Constraint due to gravitational waves observations is also shown (green arrow).

Chapter 5

Conclusions

The development of a numerical Python code capable of solving the TOV equations has allowed us to make predictions for the maximum mass and radius of neutron stars, which have been subsequently compared to astrophysical observations. These results are based on a Skyrme-EDF model conceived for cold ($T = 0$) and static (non-rotating) neutron stars without hyperons or other degrees of freedom different than nucleons, electrons and muons in the inner core.
The general idea was to build a code in several steps, progressively introducing improvements and testing certain variables such as the exit pressure and the quadratic approximation to the energy per nucleon. First, it has been tested with Skyrme models that had already been widely used in literature to verify that it gave compatible results. Then, the new code was used by implementing functionals not yet used in literature for calculations of neutron stars masses, radii. We have also computed an additional quantity, namely the tidal deformability.

We have considered the equation of state derived from Skyrme-type interactions within the framework of mean field theories. We have merged this EoS with the BPS one at low density and we have extrapolated such EoS for all densities higher than those included in the BPS model, despite the parameters of the various Skyrme interactions are fitted at values around ρ_0, and therefore, a priori, it is not possible to know if they also work at higher densities.
We have first considered a matter composed solely of neutrons, protons, and electrons that satisfies the conditions of beta-equilibrium and zero net charge. This allowed us to calculate the fraction of each particle type over the total number of baryons for a certain value of density. Then, by using the expression for the energy per nucleon derived from a Skyrme-type model and treating the electrons as an ideal gas of ultra-relativistic fermions, we have been able to calculate the total energy density and pressure values for each density and then build a part of the overall equation of state.
The next step would have been to interface the BPS equation of state with the newly constructed one. With appropriate considerations on merging, which in particular had to be done in such a way as to preserve causality, an overall EoS for *npe* matter was obtained. With it, we solved the TOV equations to obtain a first set of results of mass and radius for neutron stars.

Table 5.1: Maximum masses as predicted by SAMi-J models. In the last column, the values of maximum mass scaled with a qualitative percentage of 4% for rotation effects are reported.

Skyrme	$\mathbf{M}_{max}$ [$M_\odot$]	**Rescaled** $\mathbf{M}_{max}$ [$M_\odot$]
SAMi-J29	2.10	2.18
SAMi-J30	2.14	2.22
SAMi-J31	2.17	2.26
SAMi-J32	2.18	2.27
SAMi-J33	2.19	2.28
SAMi-J34	2.19	2.28
SAMi-J35	2.20	2.29

Subsequently, muons, which were initially excluded from our model, were implemented in the code. The matter formed by protons, neutrons, electrons, and muons must still satisfy the conditions of beta-equilibrium and neutral charge. Muons emerge only starting from a certain density, at which point they become energetically favored in the system compared to electrons. From the results, it has been observed that this threshold density is model-dependent, but on average it is around 0.11 fm^{-3}. It has also been noted that there are Skyrme parameterizations for which the fraction of muons assumes a significant weight in the balance of particles present (e.g. SkI3), while for others their percentage remains low (e.g. SLy4). Therefore, the addition of muons in our model has more or less significant consequences on mass-radius relation depending on the Skyrme used.

Finally, we used the new code to calculate mass-radius diagrams for the Skyrme SAMi-J models. The results obtained are consistent with NICER observations and gravitational wave detections, but only the SAMi-J33, SAMi-J34, and SAMi-J35 models satisfy the most recent constraint for the heaviest observed neutron star. However, it should be noted that this neutron star also has the highest spin observed, so by adding a qualitative correction for rotation to our model (which would roughly affect the mass by 3% to 4%, as seen in article [60]), we could potentially explain discrepancies for the other SAMi-J models as well. Table 5.1 reports the maximum masses predicted by the various Skyrme models, along with their values potentially scaled up by 4%. It is important to note that the effects of rotation may vary depending on the model, and therefore our estimate is not intended to provide an ultimate response.

We have also implemented the Fayans functional and calculated its predictions for mass and radius values of neutron stars. However, the results show a strong disagreement with all astrophysical observations. Although this functional has a good predictive power in nuclear-structure calculations, it has been found to be ineffective in reproducing results consistent with observations for neutron stars. It should be noted that the Fayans functional was a priori constructed with the idea of describing matter in a range of high densities, such as those encountered in neutron stars. This conclusion refers to the original functional proposed by Fayans: however, there are currently optimized Fayans functionals that were not considered in this work[61].

Finally, we calculated the tidal deformability; the results for the parameter Λ were calculated with the same functionals used for mass and radius calculations. In this case only the SAMi-J35 functional does not meet the constraint imposed by the GW170817 event of a $\Lambda_{1.4} < 800$ for a star of mass 1.4 times that of the Sun.

Bibliography

[1] L. D. Landau, "On the theory of stars," *Phys. Z. Sowjetunion*, vol. 285, 1932.

[2] D. G. Yakovlev, P. Haensel, G. Baym, and C. Pethick, "Lev landau and the concept of neutron stars," *Physics-Uspekhi*, vol. 56, pp. 289–295, mar 2013.

[3] M. C. Miller, F. K. Lamb, A. J. Dittmann, S. Bogdanov, Z. Arzoumanian, K. C. Gendreau, S. Guillot, A. K. Harding, W. C. G. Ho, J. M. Lattimer, R. M. Ludlam, S. Mahmoodifar, S. M. Morsink, P. S. Ray, T. E. Strohmayer, K. S. Wood, T. Enoto, R. Foster, T. Okajima, G. Prigozhin, and Y. Soong, "PSR j00300451 mass and radius from iNICER/i data and implications for the properties of neutron star matter," *The Astrophysical Journal*, vol. 887, p. L24, dec 2019.

[4] T. E. Riley, A. L. Watts, P. S. Ray, S. Bogdanov, S. Guillot, S. M. Morsink, A. V. Bilous, Z. Arzoumanian, D. Choudhury, J. S. Deneva, K. C. Gendreau, A. K. Harding, W. C. G. Ho, J. M. Lattimer, M. Loewenstein, R. M. Ludlam, C. B. Markwardt, T. Okajima, C. Prescod-Weinstein, R. A. Remillard, M. T. Wolff, E. Fonseca, H. T. Cromartie, M. Kerr, T. T. Pennucci, A. Parthasarathy, S. Ransom, I. Stairs, L. Guillemot, and I. Cognard, "A NICER view of the massive pulsar PSR j07406620 informed by radio timing and XMM-newton spectroscopy," *The Astrophysical Journal Letters*, vol. 918, p. L27, sep 2021.

[5] F. J. Fattoyev, J. Piekarewicz, and C. J. Horowitz, "Neutron skins and neutron stars in the multimessenger era," *Phys. Rev. Lett.*, vol. 120, p. 172702, Apr 2018.

[6] R. W. Romani, D. Kandel, A. V. Filippenko, T. G. Brink, and W. Zheng, "PSR j0952-0607: The fastest and heaviest known galactic neutron star," *The Astrophysical Journal Letters*, vol. 934, p. L17, jul 2022.

[7] B. P. Abbott, R. Abbott, T. D. Abbott, *et al.*, "Gw170817: Observation of gravitational waves from a binary neutron star inspiral," *Phys. Rev. Lett.*, vol. 119, p. 161101, Oct 2017.

[8] G. E, "Neutron stars set to open their heavy hearts," *Nature*, vol. 546, 2017.

[9] J. Piekarewicz, "The nuclear physics of neutron stars," 2022.

[10] P. Haensel, A. Y. Potekhin, and D. G. Yakovlev, *Neutron Stars 1: Equation of State and Structure*. 2007.

[11] G. Baym, C. J. Pethick, and P. G. Sutherland, "The ground state of matter at high densities: Equation of state and stellar models," *The Astrophysical Journal*, vol. 170, pp. 299–317, 1971.

[12] I. Bombaci, “The hyperon puzzle in neutron stars,” in *Proceedings of the 12th International Conference on Hypernuclear and Strange Particle Physics (HYP2015)*, Journal of the Physical Society of Japan, jul 2017.

[13] D. Logoteta, “Hyperons in neutron stars,” *Universe*, vol. 7, no. 11, 2021.

[14] M. Kramer, *Pulsar Timing as an Exoplanet Discovery Method*, pp. 1–20. Cham: Springer International Publishing, 2017.

[15] F. Özel, D. Psaltis, S. Ransom, P. Demorest, and M. Alford, “THE MASSIVE PULSAR PSR j1614–2230: LINKING QUANTUM CHROMODYNAMICS, GAMMA-RAY BURSTS, AND GRAVITATIONAL WAVE ASTRONOMY,” *The Astrophysical Journal*, vol. 724, pp. L199–L202, nov 2010.

[16] T. E. Riley, A. L. Watts, S. Bogdanov, P. S. Ray, R. M. Ludlam, S. Guillot, Z. Arzoumanian, C. L. Baker, A. V. Bilous, D. Chakrabarty, K. C. Gendreau, A. K. Harding, W. C. G. Ho, J. M. Lattimer, S. M. Morsink, and T. E. Strohmayer, “A iNICER/i view of PSR j00300451: Millisecond pulsar parameter estimation,” *The Astrophysical Journal*, vol. 887, p. L21, dec 2019.

[17] A. Bauswein, O. Just, H.-T. Janka, and N. Stergioulas, “Neutron-star radius constraints from gw170817 and future detections,” *The Astrophysical Journal Letters*, vol. 850, p. L34, nov 2017.

[18] R. Essick, I. Tews, P. Landry, S. Reddy, and D. E. Holz, “Direct astrophysical tests of chiral effective field theory at supranuclear densities,” *Phys. Rev. C*, vol. 102, p. 055803, Nov 2020.

[19] R. Essick, I. Tews, P. Landry, S. Reddy, and D. E. Holz, “Direct astrophysical tests of chiral effective field theory at supranuclear densities,” *Phys. Rev. C*, vol. 102, p. 055803, Nov 2020.

[20] J. R. Oppenheimer and G. M. Volkoff, “On massive neutron cores,” *Phys. Rev.*, vol. 55, pp. 374–381, Feb 1939.

[21] S. Carroll, *Spacetime and Geometry: An Introduction to General Relativity.* 2019.

[22] S. Shapiro and S. Teukolsky, *Black Holes, White Dwarfs, and Neutron Stars: The Physics of Compact Objects.* 1983.

[23] K. Chatziioannou, “Neutron-star tidal deformability and equation-of-state constraints,” *General Relativity and Gravitation*, vol. 52, nov 2020.

[24] E. Poisson, *Gravity: Newtonian, Post-Newtonian, Relativistic.* 2014.

[25] T. Hinderer, “Tidal love numbers of neutron stars,” *The Astrophysical Journal*, vol. 677, pp. 1216–1220, apr 2008.

[26] K. . C. A. Thorne, “Non-radial pulsation of general-relativistic stellar models. i. analytic analysis for l $>=$ 2,” vol. 149, p. 591, 1967.

[27] C. Moustakidis, “Nuclear equation of state constraints from tidal deformability of neutron stars,” *HNPS Proceedings*, vol. 21, p. 44, 03 2019.

[28] L. Blanchet, "Gravitational radiation from post-newtonian sources and inspiralling compact binaries," *Living Reviews in Relativity*, vol. 17, feb 2014.

[29] Z. Carson, K. Chatziioannou, C.-J. Haster, K. Yagi, and N. Yunes, "Equation-of-state insensitive relations after GW170817," *Physical Review D*, vol. 99, apr 2019.

[30] C. F. v. Weizsäcker, "Zur theorie der kernmassen," vol. 96, pp. 431–458, 1935.

[31] A. H. Wapstra, *Atomic Masses of Nuclides*, pp. 1–37. Berlin, Heidelberg: Springer Berlin Heidelberg, 1958.

[32] J. Rohlf, *Modern Physics from A to Z.* 1994.

[33] D. Benzaid *et al.*, "Bethe–weizsäcker semiempirical mass formula coefficients 2019 update based on ame2016," *Nuclear Science and Techniques*, 2020.

[34] T. Skyrme, "The effective nuclear potential," *Nuclear Physics*, vol. 9, no. 4, pp. 615–634, 1958.

[35] J. Rikovska Stone, J. C. Miller, R. Koncewicz, P. D. Stevenson, and M. R. Strayer, "Nuclear matter and neutron-star properties calculated with the skyrme interaction," *Phys. Rev. C*, vol. 68, p. 034324, Sep 2003.

[36] D. Vautherin and D. M. Brink, "Hartree-fock calculations with skyrme's interaction. i. spherical nuclei," *Phys. Rev. C*, vol. 5, pp. 626–647, Mar 1972.

[37] B.-A. Li, B.-J. Cai, L.-W. Chen, and J. Xu, "Nucleon effective masses in neutron-rich matter," *Progress in Particle and Nuclear Physics*, vol. 99, pp. 29–119, mar 2018.

[38] B.-A. Li, B.-J. Cai, L.-W. Chen, and J. Xu, "Nucleon effective masses in neutron-rich matter," *Progress in Particle and Nuclear Physics*, vol. 99, pp. 29–119, mar 2018.

[39] Z. Zhang and L.-W. Chen, "Constraining the symmetry energy at subsaturation densities using isotope binding energy difference and neutron skin thickness," *Physics Letters B*, vol. 726, pp. 234–238, oct 2013.

[40] B.-J. Cai and L.-W. Chen, "Constraints on the skewness coefficient of symmetric nuclear matter within the nonlinear relativistic mean field model," *Nuclear Science and Techniques*, vol. 28, dec 2017.

[41] C.-H. Lee, T. T. S. Kuo, G. Q. Li, and G. E. Brown, "Nuclear symmetry energy," *Phys. Rev. C*, vol. 57, pp. 3488–3491, Jun 1998.

[42] M. Baldo and G. Burgio, "The nuclear symmetry energy," *Progress in Particle and Nuclear Physics*, vol. 91, pp. 203–258, nov 2016.

[43] S. A. Fayans, "Towards a universal nuclear density functional," vol. 68, pp. 169–174, 1998.

[44] B. Friedman and V. Pandharipande, "Hot and cold, nuclear and neutron matter," *Nuclear Physics A*, vol. 361, no. 2, pp. 502–520, 1981.

[45] R. B. Wiringa, V. Fiks, and A. Fabrocini, "Equation of state for dense nucleon matter," *Phys. Rev. C*, vol. 38, pp. 1010–1037, Aug 1988.

[46] C. Pethick, "Dense matter and neutron stars: Some basic notions," *Acta Physica Polonica B*, vol. 50, no. 12, p. 2145, 2019.

[47] R. R. Silbar and S. Reddy, "Neutron stars for undergraduates," *American Journal of Physics*, vol. 72, pp. 892–905, jul 2004.

[48] J. R. Oppenheimer and G. M. Volkoff, "On massive neutron cores," *Phys. Rev.*, vol. 55, pp. 374–381, Feb 1939.

[49] M. G. Alford and S. P. Harris, "β equilibrium in neutron-star mergers," *Phys. Rev. C*, vol. 98, p. 065806, Dec 2018.

[50] S. Reddy, M. Prakash, and J. M. Lattimer, "Neutrino interactions in hot and dense matter," *Phys. Rev. D*, vol. 58, p. 013009, May 1998.

[51] C.-J. Jiang, Y. Qiang, D.-W. Guan, Q.-Z. Chai, C.-Y. Qiao, and J.-C. Pei, "From finite nuclei to neutron stars: The essential role of high-order density dependence in effective forces," *Chinese Physics Letters*, vol. 38, p. 052101, jun 2021.

[52] G. Baym, H. A. Bethe, and C. J. Pethick, "Neutron star matter," *Nuclear Physics A*, vol. 175, no. 2, pp. 225–271, 1971.

[53] M. Fortin, C. Providê ncia, A. R. Raduta, F. Gulminelli, J. L. Zdunik, P. Haensel, and M. Bejger, "Neutron star radii and crusts: Uncertainties and unified equations of state," *Physical Review C*, vol. 94, sep 2016.

[54] X. Roca-Maza, G. Colò, and H. Sagawa, "New skyrme interaction with improved spin-isospin properties," *Phys. Rev. C*, vol. 86, p. 031306, Sep 2012.

[55] X. Roca-Maza, M. Brenna, B. K. Agrawal, P. F. Bortignon, G. Colò, L.-G. Cao, N. Paar, and D. Vretenar, "Giant quadrupole resonances in ^{208}pb, the nuclear symmetry energy, and the neutron skin thickness," *Phys. Rev. C*, vol. 87, p. 034301, Mar 2013.

[56] D. Blaschke, D. E. Alvarez-Castillo, and T. Klahn, "Universal symmetry energy contribution to the neutron star equation of state," 2016.

[57] F. Sammarruca, "The symmetry energy: Current status of ab initio predictions vs. empirical constraints," 2022.

[58] J.-P. Lasota, P. Haensel, and M. A. Abramowicz, "Fast rotation of neutron stars," *The Astrophysical Journal*, vol. 456, p. 300, jan 1996.

[59] O. Benhar, V. Ferrari, L. Gualtieri, and S. Marassi, "Perturbative approach to the structure of rapidly rotating neutron stars," *Physical Review D*, vol. 72, aug 2005.

[60] P. S. Koliogiannis and C. C. Moustakidis, "Effects of the equation of state on the bulk properties of maximally rotating neutron stars," *Phys. Rev. C*, vol. 101, p. 015805, Jan 2020.

[61] P.-G. Reinhard and W. Nazarewicz, "Toward a global description of nuclear charge radii: Exploring the fayans energy density functional," *Physical Review C*, vol. 95, jun 2017.